

Field test of the JNIOSH Mini Pipe Strain Meter as a safety alert system during trench work

André Lan
Bertrand Galy
Satoshi Tamate
Tomohito Hori
Nabutaka Hiraoka

STUDIES AND
RESEARCH PROJECTS

R-1124-en

OUR RESEARCH is working for you !

The Institut de recherche Robert-Sauvé en santé et en sécurité du travail (IRSST), established in Québec since 1980, is a scientific research organization well-known for the quality of its work and the expertise of its personnel.

Mission

To contribute, through research, to the prevention of industrial accidents and occupational diseases and to the rehabilitation of affected workers;

To disseminate knowledge and serve as a scientific reference centre and expert;

To provide the laboratory services and expertise required to support the public occupational health and safety network.

Funded by the Commission des normes, de l'équité, de la santé et de la sécurité du travail, the IRSST has a board of directors made up of an equal number of employer and worker representatives.

To find out more

Visit our Web site for complete up-to-date information about the IRSST. All our publications can be downloaded at no charge.

www.irsst.qc.ca

To obtain the latest information on the research carried out or funded by the IRSST, subscribe to our publications:

- *Prévention au travail*, the free magazine published jointly by the IRSST and the CNESST (preventionautravail.com)
- [InfoIRSST](#), the Institute's electronic newsletter

Legal Deposit

Bibliothèque et Archives nationales du Québec, 2022
ISBN 978-2-89797-151-9 (PDF)

© Institut de recherche Robert-Sauvé en santé et en sécurité du travail, 2022

IRSST – Communications, Strategic Watch
and Knowledge Mobilization Division
505 De Maisonneuve Blvd. West
Montréal, Québec
H3A 3C2
Phone: 514 288-1551
publications@irsst.qc.ca
www.irsst.qc.ca

Field test of the JNIOOSH Mini Pipe Strain Meter as a safety alert system during trench work

André Lan¹, Bertrand Galy¹,
Satoshi Tamate², Tomohito Hori², Nabutaka Hiraoka²

1. IRSST
2. National Institute of Occupational Safety and Health,
Japan (JNIOOSH)



Disclaimer

The IRSST makes no guarantee as to the accuracy, reliability or completeness of the information in this document.

Under no circumstances may the IRSST be held liable for any physical or psychological injury or material damage resulting from the use of this information.

Document content is protected by Canadian intellectual property legislation.

A PDF version of this publication is available on the IRSST Web site.

STUDIES AND
RESEARCH PROJECTS

R-1124-en





PEER REVIEW

In compliance with IRSST policy, the research results published in this document have been peer-reviewed.

ACKNOWLEDGMENTS

This expertise was made possible by the cooperation and support of a number of organizations, collaborators and specialists in construction and occupational health and safety. We especially thank the following organization and individuals:

- The Quebec Ministry of Transport, Sustainable Mobility and Transport Electrification (MTMDET) for providing the Louiseville site for our field test;
- Sophie Rainville, Olivier Hamelin, Maxime Bolduc, Antony Gagné and René Milette for their help, support, availability and collaboration in facilitating our access to the site and allowing us to carry out the field tests under favorable conditions;
- Naotaka Kikkawa from the National Institute of Occupational Safety and Health, Japan (JNIOOSH) for his support from Tokyo while the experimental program was taking place in Quebec.

ABSTRACT

Trenching work exposes workers to many risks. Cave-in is the most serious and frequent risk during such work, but unfortunately, it is very often underestimated, as even a minor or partial cave-in of less than 1 m³ of soil can fatally injure a worker. An analysis of 59 reports of serious and fatal accidents in excavation and trenching work from the Commission des normes, de l'équité, de la santé et de la sécurité du travail (CNESST), between June 1973 and May 2015, shows that there were 51 fatalities and 25 serious accidents in Quebec. Wall collapses frequently cause occupational accidents on construction sites and must be avoided at all costs. In order to do this, slopes must be excavated at a safe angle, depending on the type of soil, or temporary retaining walls must be erected to support the slopes.

Cave-in accidents are a reminder that the shear strength of natural soil deposits is not uniform and that trench stability varies from one point to another within a deposit. Although Occupational Safety and Health Administration (OSHA) regulations, Health and Safety at Work regulations and various Canadian provincial regulations prescribe maximum allowable slopes for safe excavations, there is always a risk of landslide in an embankment.

Cave-ins occur frequently on small construction projects and cause fatalities and/or serious accidents. Many of these fatalities and serious injuries could have been avoided if the workers had identified the warning signs of a cave-in and had therefore been able to evacuate the excavation in time. Case studies reveal that workers do not always have time to evacuate the excavation because 1) the time between the completion of the excavation and the onset of the cave-in causes the workers to misinterpret the stability of the soil mass, 2) creep phenomena occur before the cave-in and 3) ground movements are initially too small to be detected by simple observation.

Indeed, wall failure is very difficult to predict by visual observation alone. Monitoring sensors can be used to identify small movements in a slope or wall, indicating an increased risk of cave-in, and warn workers of the imminent risk. They can then evacuate the excavation in time to avoid serious accidents or fatalities. Given the environment in which these monitoring sensors are used temporarily on construction sites, they must be quick to install and easy to use.

The Mini Pipe Strain Meter (MPSM) was previously developed at the National Institute of Occupational Safety and Health, Japan (JNIOOSH) and was tested in their laboratory with Japanese soils to measure the increase in shear strain in the shallow subsoil of embankments. An increase in strain indicates an impending cave-in and the MPSM emits sound and light signals to warn workers in time to evacuate the trench.

Full-scale model tests of slope and wall failure performed in the laboratory at the JNIOOSH showed that:

- 1) The MPSM detected the risk of slope failure for those tests;
- 2) Small shear deformations at shallow depths were clearly mobilized, which corresponded to the development of sliding surfaces in deeper parts;
- 3) The identification of the second or third creep could give workers a few minutes to evacuate;

- 4) When the risk of slope failure or wall cave-in increases, it is not perceptible by observation alone;
- 5) No visible cracks were observed during the tests and no ground movements were visible before the failure;
- 6) The length of time before failure depended on the soil and on the excavation conditions;
- 7) The cave-in of a slope or wall can be predicted by measurement; therefore, the risk can be detectable by prediction.

By warning that a collapse is imminent, the MPSM helps reducing the risk of injury from cave-in. In short, the MPSM is not a system for preventing slope or wall to cave-in, but rather a method for monitoring the risks. Other safety measures should be used in conjunction with the MPSM.

As the MPSM was developed and successfully tested to monitor trench stability and wall collapse in typical soils of Japan, its performance with other types of soil remained unknown. Therefore, the focus of the present expertise was to determine whether the MPSM would perform effectively *in situ* in sensitive clay, a typical soil of the Champlain Sea, which makes up the subsurface of more than 80% of the inhabited territory of the province of Quebec. This expertise was possible as a larger study entitled *Soil classification and selection of shoring systems for the excavation of trenches (IRSST Project #0099-5290)* was concomitantly realized.

The tests results showed that:

- The MPSM is easy to install manually on site with a wrench key;
- The MPSM worked well during site tests in typical Champlain Sea clay;
- During these tests, the first warning signal (D1: yellow light) and the second warning signal (D2: red light) were triggered, indicating an imminent cave-in. D1 lasted 22 minutes, whereas D2 lasted 50 seconds;
- The MPSM provided a means of measuring any increase in the risk of a cave-in during trench excavation;
- The MPSM has potential for use on Quebec sites of Champlain clay if it is available at a reasonable price. It currently sells for about US\$7,000 in Japan.

Further testing of the MPSM is nonetheless required with other types of Quebec soil and to assess its reliability and sensitivity regarding the influence of its placement with respect to the trench or slope.

TABLE OF CONTENTS

ACKNOWLEDGMENTS	i
ABSTRACT	iii
LIST OF TABLES	vii
LIST OF FIGURES	ix
LIST OF ACRONYMS	xi
1. INTRODUCTION	1
1.1 Slope monitoring devices	1
1.2 Mini Pipe Strain Meter	3
2. MPSM TECHNOLOGY DEVELOPMENT AT JNIOOSH	5
2.1 Trench failure prediction by shear strain in shallow subsurfaces	5
2.2 MPSM description and installation	5
2.3 Laboratory experiment with the MPSM	7
2.3.1 Preparation of a full-scale slope model.....	7
2.3.2 Experimental analysis of movement near the shoulder	12
2.3.3 Discussion	14
2.4 Conclusions of laboratory experiment	16
3. OBJECTIVE	19
4. METHODOLOGY	21
4.1 Louiseville test site	21
4.2 Experimental field tests	23
4.3 Site layout and instrumentation	24
4.3.1 Trench A1	24
4.3.2 Trench A2	27
5. OBSERVATIONS AND RESULTS	35
5.1 Weather monitoring during tests.....	35
5.2 Trench A1.....	35
5.2.1 Observations and behaviour of trench A1 as excavation progressed – May 8, 2018	35
5.2.2 Piezometer data.....	37
5.2.3 Inclinometer data	38
5.2.4 MPSM data	40

5.3	Trench A2	41
5.3.1	Piezometer data	41
5.3.2	Inclinometers results	41
5.3.3	MPSM data with loading of concrete blocks	43
6.	ANALYSIS AND INTERPRETATION OF MPSM DATA FOR TRENCH A1	49
7.	CONCLUSION AND LIMITATIONS	53
	REFERENCES	55

LIST OF TABLES

Table 1.	Soil properties of Kanto loam	7
Table 2.	Conditions of static compression using construction machinery	8
Table 3.	Sensor characteristics	9
Table 4.	Geotechnical properties of Louiseville soils for a 200 mm sample.....	21
Table 5.	Experimental tests characteristics for sensitive clay soil	23
Table 6.	Test site instrumentation and geotechnical tests.....	24
Table 7.	Meteorological observations at Louiseville for summer of 2018.....	35
Table 8.	Timeline of notable events during loading of trench A2 with concrete blocks on Day 1 (August 6, 2018)	44
Table 9.	Timeline of notable events during loading of trench A2 with concrete blocks on Day 2 (August 7, 2018)	45

LIST OF FIGURES

Figure 1.	Distribution of strain in the horizontal direction, as computed from the finite element model analysis.	5
Figure 2.	Mini Pipe Strain Meter (MPSM) system.....	6
Figure 3.	Installation of the MPSM by use of a hand-operated drill in less than 10 seconds.	6
Figure 4.	Static compression of the soil material using an excavator for the preparation of the slope model.	7
Figure 5.	Progression of the excavation, which eventually caused instability of the slope.....	9
Figure 6.	Installation of DTPs to measure surface settlement near the shoulder.	10
Figure 7.	Position of installed sensors and parts of excavation shown with (a) a profile view and (b) a plane view.	11
Figure 8.	Process of failure of excavated wall in five seconds.	12
Figure 9.	Profile shape of slope before and after excavation, and after failure.	12
Figure 10.	Reaction of DTP, ASG and MPSM sensors prior to failure.	13
Figure 11.	Inverse of velocity of shear strain as provided by MPSM1.....	15
Figure 12.	Location of the municipality of Louiseville in relation to the Champlain Sea (Mer de Champlain) and the Laflamme Sea (Golfe de Laflamme).....	21
Figure 13.	Undrained shear strength (S_u) and residual undrained shear strength (S_{ur}) of Louiseville clay.	22
Figure 14.	Trench layout.....	23
Figure 15.	Plane view (top) and profile view (bottom) of trench A1, 10 m long, 8.75 m wide and 5 m deep, with 1 vertical wall and 1 benched wall.	25
Figure 16.	Excavation of trench A1.	26
Figure 17.	Excavation procedures for trench A1.	27
Figure 18.	Plane view (top) and profile view (bottom) of trench A2, 10 m long, about 20 m wide and about 4.2 m deep, with a 1.6:1 wall and a benched wall.....	28
Figure 19.	Trench A2 with a rectangular pattern marked with orange paint to monitor ground movement.	29
Figure 20.	Digging of trench A2 with Caterpillar 315 and Caterpillar 320 excavators.	29
Figure 21.	Excavation procedures for trench A2.	30
Figure 22.	Progression of trench A2 as excavation was carried out.....	31
Figure 23.	Loading of trench A2 with concrete blocks.....	31
Figure 24.	First loading pattern of trench A2 with concrete blocks.....	32

Figure 25.	Second loading pattern of trench A2 with concrete blocks.....	32
Figure 26.	Loading of trench A2 with concrete blocks and sand.	33
Figure 27.	Additional loading of trench A2 with sand.....	33
Figure 28.	Rupture due to flaking and water inflow during excavation of trench A1 (step 3).	36
Figure 29.	Rupture of vertical wall at a depth of 5 m, carrying the MPSM to bottom of the trench.	36
Figure 30.	Major block of soil broke away, causing the wall to recede by 1.75 m.	37
Figure 31.	Piezometer results for trench A1, during excavation on May 8, 2018.	37
Figure 32.	Vertical inclinometer VI-A1.1 (left = ΔX , right = ΔY , results in mm).	38
Figure 33.	Vertical inclinometer VI-A1.2 (left = ΔX , right = ΔY , results in mm).	39
Figure 34.	Horizontal inclinometer HI-A1.3 (results in mm).	39
Figure 35.	Flashing yellow light of D1 warning, following the detection of the second creep phenomenon prior to failure.....	40
Figure 36.	Flashing red light of D2 warning, following the detection of the third creep phenomenon prior to failure.	40
Figure 37.	Results of the piezometers A2.1, A2.2 and A2.3 for the period from May 5 to August 11, 2018.	41
Figure 38.	Vertical inclinometer results (VI-A2) for trench A2 (left = ΔX , right = ΔY , results in mm).	42
Figure 39.	Horizontal inclinometer (HI-A2) results for trench A2 (results in mm).	42
Figure 40.	MPSM results during trench A2 loading, showing two specific loading periods (Day 1 and Day 2).	46
Figure 41.	MPSM results during first loading of trench A2 with concrete blocks, showing the effect of placing blocks in the close vicinity of the device.....	46
Figure 42.	Inverse of shear strain rate $ 1/v_\theta $ as a function of time for trench A2 during the first loading with concrete blocks (Day 1).	47
Figure 43.	MPSM results during second loading of trench A2 with concrete blocks and sand.....	47
Figure 44.	Relationship between interpreted shear strain θ and the entire elapsed time.....	49
Figure 45.	Expanded view of relationship between θ and the elapsed time (t_e) prior to failure.....	50
Figure 46.	Relationship between inverse of shear strain rate $ 1/v_\theta $ and entire elapsed time t_e	51
Figure 47.	Expanded view of relationship between the inverse shear strain ($ 1/v_\theta $) and the remaining time prior to failure (t_r), for 80 minutes prior to failure (left panel) and for 25 minutes prior to failure (right panel).....	52

LIST OF ACRONYMS

ALS:	Airborne Laser Scanner
CNESST:	Commission des normes, de l'équité, de la santé et de la sécurité du travail
ÉTS:	École de Technologie Supérieure
FEM:	Finite Element Model
GB-InRAR:	Ground-Based Interferometric Real Aperture Radar
HRDEM:	High Resolution Digital Elevation Model
InSAR:	Interferometric Synthetic Aperture Radar
IRSST:	Institut de recherche Robert-Sauvé en santé et en sécurité du travail
JNIOOSH:	National Institute of Occupational Safety and Health, Japan
LiDAR:	Light Detection and Ranging
LU:	Laval University
MPSM:	Mini Pipe Strain Meter
MTMDET:	Quebec Ministry of Transport, Sustainable Mobility and Transport Electrification
OSHA:	Occupational Safety and Health Administration
RPAS:	Remotely Piloted Aircraft Systems
SSMR:	Slope Stability Mining Radar
TLS:	Terrestrial Laser Scanner

1. INTRODUCTION

Trenching work exposes workers to many risks. Cave-in is the most serious and frequent risk during such work. Unfortunately, it is very often underestimated as even a minor or partial cave-in of less than 1 m³ of soil can fatally injure a worker. An analysis of 59 reports of serious and fatal accidents in excavation and trenching work from the Commission des normes, de l'équité, de la santé et de la sécurité du travail (CNESST) between June 1973 and May 2015 shows that there were 51 fatalities and 25 serious accidents in Quebec (Lan, s.d.). Wall collapses frequently cause occupational accidents on construction sites and must be avoided at all costs. In order to do this, slopes must be excavated at a safe angle, depending on the type of soil, or temporary retaining walls must be erected to support the slopes.

Cave-in accidents are a reminder that the shear strength of natural soil deposits is not uniform and that trench stability varies from one point to another within a deposit. Although Occupational Safety and Health Administration (OSHA) regulations (1989a, 1989b, 1989c, 1994), Health and Safety at Work regulations (Health and Safety Executive [HSE], 1974) and various Canadian provincial regulations (en Alberta, *Occupational Health and Safety Act*; en Colombie-Britannique, *Occupational Health and Safety Regulation*; en Ontario, *Construction Projects*) prescribe maximum allowable slopes for safe excavations, there is always a risk of landslide in an embankment.

Cave-ins occur frequently on small construction projects and cause fatalities and/or serious accidents (Tamate & Hori, 2017). Many of these fatalities and serious injuries could have been avoided if the workers had identified the warning signs of a cave-in and had therefore been able to evacuate the excavation in time. Case studies reveal that workers do not always have time to evacuate the excavation because 1) the time between the completion of the excavation and the onset of the cave-in causes the workers to misinterpret the stability of the soil mass, 2) creep phenomena occur before the cave-in and 3) ground movements are initially too small to be detected by simple observation.

Indeed, wall failure is very difficult to predict by visual observation alone. Monitoring sensors can be used to identify small movements in the slope or wall, indicating an increased risk of cave-in, and warn workers of the imminent risk. They can then evacuate the excavation in time to avoid serious accidents or fatalities. Given the environment in which these monitoring devices are used temporarily on construction sites, they must be quick to install and easy to use.

1.1 Slope monitoring devices

In the last decade, different technologies have been developed to monitor slope movements and to try to predict failures (Wang, Liu, Yang, & Xie, 2017). Among those technologies, we can list (Jaboyedoff et al., 2012; Kovacevic et al., 2018; Kumar & Villuri, 2015; Wang et al., 2017):

- Interferometric Synthetic Aperture Radar (InSAR);
- Ground-Based Interferometric Real Aperture Radar (GB-InRAR);

- Light Detection And Ranging (LiDAR), based either on Terrestrial Laser Scanner (TLS) or Airborne Laser Scanner (ALS);
- Remotely Piloted Aircraft Systems (RPAS);
- High-resolution photogrammetry;
- Slope Stability Mining Radar (SSMR).

InSAR and LiDAR are the two techniques that are widely used for landslide investigations. They can also be used for other applications such as (i) detection and characterization of mass movements; (ii) hazard assessment and susceptibility mapping; (iii) slope modelling and (iv) slope monitoring (Jaboyedoff et al., 2012). These two methods can be used to gather data to be input in 2D or 3D finite element models (FEM) or high resolution digital elevation models (HRDEMs). Following the generation of these models, landslide susceptibility can be assessed. However, the resolution for this kind of prediction is generally high (1 m).

With the LiDAR technology, the typical accuracy of the laser is ± 1.5 cm for a maximum distance of 800 to 1000 m (Manetti & Steinmann, 2007) in ideal conditions, but it is usually lower in real applications because of weather conditions or bad reflecting material. According to Jaboyedoff et al. (2012), “laser scanner is nowadays a common tool for displacement monitoring even if few published papers exist.” The principle behind this technology is to compute the displacement of control points between two sets of data (two epochs, gathered at different times). Jaboyedoff et al. (2012) explained that “the standard deviation of the measurements between the two epochs can be quite high, depending on multiple factors, such as the quality of the TLS data sets, the density of the points, the existence of vegetation, the roughness of the relief, the quality of the alignment between the scans, the relative or absolute position of the TLS and the variation of the surface of the terrain between the two epochs.” The standard deviation can range from 1 cm for distances less than 100 m and high point densities, to 5 cm at a distance of 100 m, as presented in a published case (Prokop & Panholzer, 2009). The TLS method is more reliable than the ALS method, although both methods require a 3D data processing software and a computer hardware, which are powerful enough to handle huge amount of data (point clouds with several millions of points) as a high point density is needed to get a good precision.

The slope stability assessment methodologies listed above still have certain limitations. Indeed, InSAR has a low temporal resolution (1/month) which makes it unsuitable for fast movements. GB-InRAR needs a line of sight, which makes it problematic for construction sites and it requires a heavy setup for real-time monitoring. LiDAR has a limited accuracy (around 1 cm for long range laboratory conditions), needs a line of sight (which can be problematic on a construction site or an urban area) and needs post processing that is quite labour intensive, which makes it unpractical for real time application (Kovacevic et al., 2018). Furthermore, Kumar and Villuri (2015) noted that laser monitoring has the same disadvantage as prism monitoring; it cannot provide early warning of failures for necessary timely actions. In their study, they used a SSMR, based on the radar technology, to monitor in real time the slope stability of open cast mines. They however reported that the SSMR system produces data for interpretation within minutes. Finally, the high-resolution photogrammetry and RPAS methodologies have limited accuracies (Kovacevic et al., 2018).

Most of the methods described above were developed for mining or for large area slope stability monitoring, where ground movements are significantly higher and develop over a longer period before failure, when compared to smaller scale slopes or trenches commonly encountered on construction sites in cities or urban areas. Some LiDAR scanners were recently developed for construction sites, such as the FARO Focus 3D S120 Laser Scanner (Kovacevic et al., 2018). However, the price of the scanner itself (around US\$15,000) and the need for specific software and computer hardware to process the data render this solution often unpractical. In addition, the processing time may be too long to predict the slope or trench wall failure before it actually occurs.

1.2 Mini Pipe Strain Meter

A few years ago, as no monitoring devices were available for cave-in detection for slopes or trenches commonly encountered on small-scale construction sites, the National Institute of Occupational Safety and Health, Japan (JNIOH) developed the Mini Pipe Strain Meter (MPSM). The MPSM was tested with Japanese soils to measure the increase in shear strain in the shallow subsoil of embankments. When an increase in strain is detected, indicating an impending cave-in, the MPSM emits sound and light signals to warn workers in time to evacuate the trench.

The next chapter describes the MPSM as it was developed at JNIOH. The objective of the current expertise, which was carried out in the Province of Quebec, is then presented in chapter 3, followed by a description of the methodology (chapter 4), a presentation of the data obtained with the MPSM in Quebec typical soils (chapter 5), a thorough analysis of these data (chapter 6) and the conclusions which can be drawn from this expertise (chapter 7).

2. MPSM TECHNOLOGY DEVELOPMENT AT JNIOSSH

2.1 Trench failure prediction by shear strain in shallow subsurfaces

JNIOSSH researchers have developed a new, simple, reliable measurement method to monitor trench stability in order to ensure safe work (Tamate & Hori, 2017). This method differs from conventional methods in soil mechanics as it uses the Mini Pipe Strain Meter (MPSM), an instrument especially designed to measure shear strain in the shallow subsurface of slopes (Tamate, 2010), areas that have been previously ignored.

A schematic view of the distribution of a strain in the horizontal direction (ϵ_x) near the shoulder of an embankment is shown in Figure 1. In this example, using finite element model (FEM) analysis, a large increase in ϵ_x appeared near the slip surface, and its increment converged with increasing distance from the slip surface. However, it seems that a small strain in the shallow subsurface was also mobilized, corresponding to the development of the slip surface.

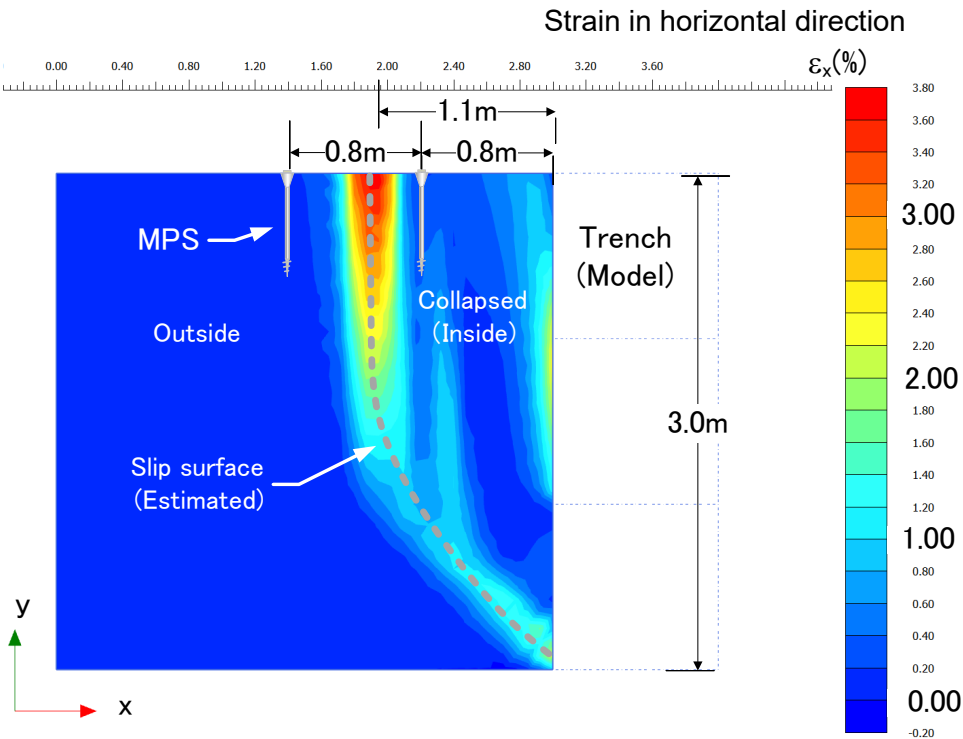


Figure 1. Distribution of strain in the horizontal direction, as computed from the finite element model analysis.

2.2 MPSM description and installation

The MPSM (Tamate & Hori, 2017; Tamate & Hori, 2018b) is made of a compact, flexible rod, 10 mm in diameter, 0.60 m long and weighing approximately 350 g (3.6 N) (Figure 2). An 80 mm long screw point, assembled at the end of the rod, allows the MPSM to penetrate the soil without

pre-boring. A 100 mm long tapered end is used to provide lateral compression to the surrounding soil so that the MPSM responds to slope movement by flexural deformation. The MPSM can be installed quickly by means of a battery-powered hand drill (Figure 3) or a manual ratchet key. The MPSM alarm system emits a sound signal to warn workers that a cave-in is imminent. One D battery cell provides the MPSM with 20-day autonomy (Figure 2).

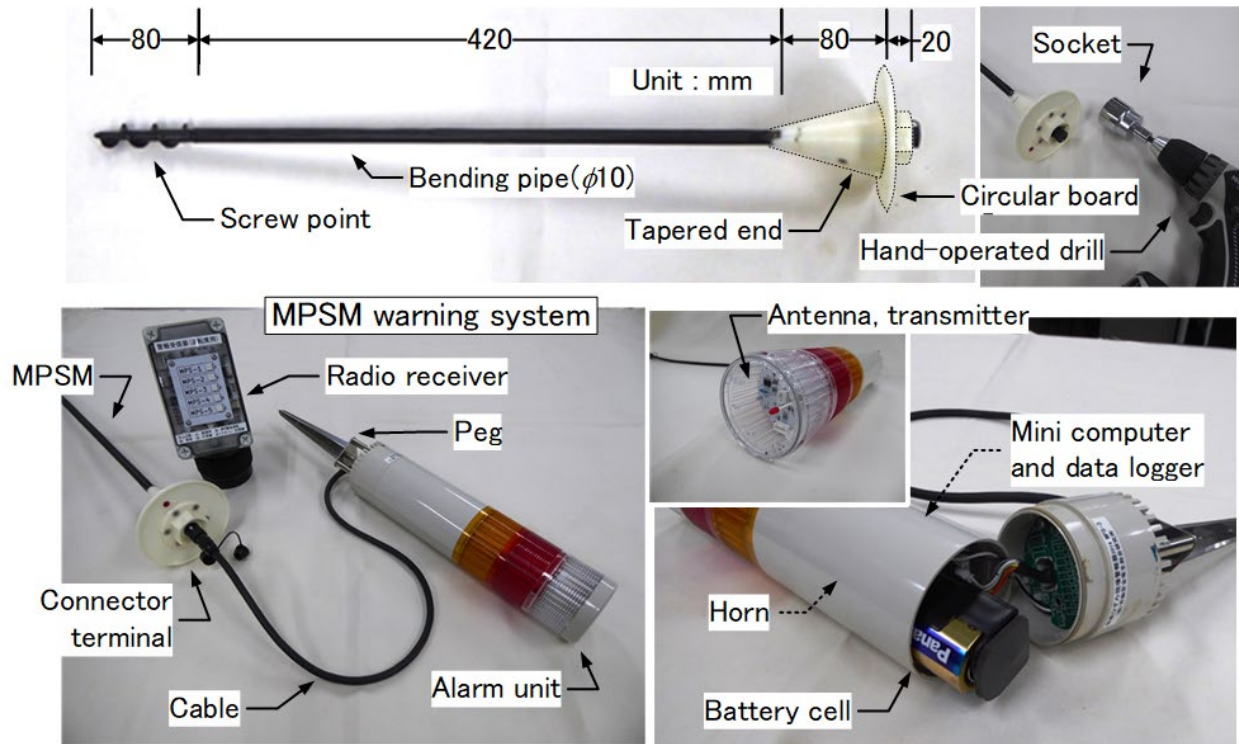


Figure 2. Mini Pipe Strain Meter (MPSM) system.



Figure 3. Installation of the MPSM by use of a hand-operated drill in less than 10 seconds.

2.3 Laboratory experiment with the MPSM

2.3.1 Preparation of a full-scale slope model

A trench failure was simulated in a slope model composed of Kanto loam, which was prepared with the optimum moisture content to represent the unsaturated condition of soil deposits in the shallow section. Table 1 shows the physical properties of Kanto loam, which is an unsaturated volcanic cohesive soil of Japan.

Table 1. Soil properties of Kanto loam

Density of soil particles ρ_s (g/cm ³)	2.759
Sand (0.075 ~ 2 mm) %	6.2
Silt (0.005 ~ 0.075 mm) %	45.3
Clay (Diameter < 0.005 mm) %	48.5
Liquid limit ω_L (%)	158.3
Plastic limit ω_p (%)	97.7
Plasticity index I_p	60.6
Dry density ρ_{dmax} (g/cm ³)	0.665
Optimum water content ω_{opt} (%)	102.0

For the preparation of the slope model, a 0.3 m layer of Kanto loam was spread over a testing surface in the laboratory (Figure 4). Static compressions were then carried out using an excavator. A slope-finishing bucket was used to apply uniform pressure on the deposited soil. A radius (R) between the bucket and the center of rotation of the upper structure of the excavator was kept at about 3.5 m so that a constant value of an acting load (F) was applied through the acting area of the bucket (A).

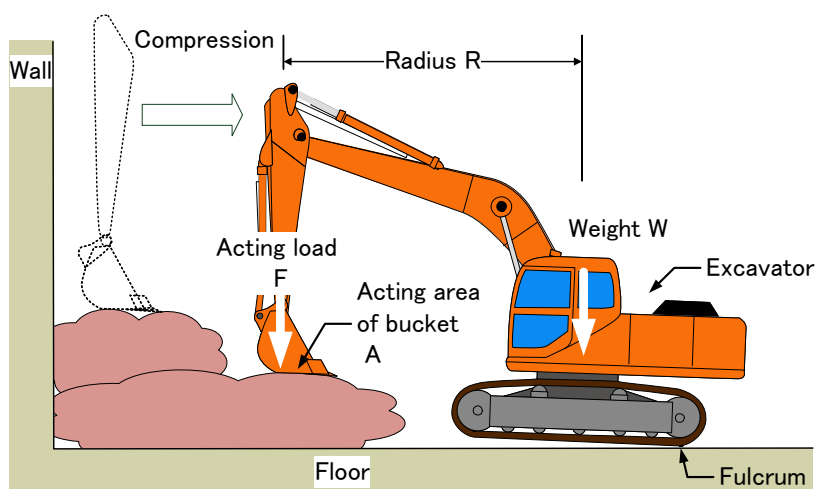


Figure 4. Static compression of the soil material using an excavator for the preparation of the slope model.

Values for the parameters for this laboratory experiment are given in Table 2. A linear relationship exists between the shear strength of soil (c) and the pressure at compression (p). The coefficient of this relationship depends on the type of soil. For the Kanto loam soil used in this laboratory experiment, this coefficient was 0.2 (Tamate Suemasa, and Katada, 2005). Thus, the relationship between c and p was derived as in equation 1:

$$c = 0.2 \times p \quad (1)$$

As a static pressure (p) of 23 kN/m² was applied by the bucket (Figure 4), a uniform shear strength of roughly 5 kN/m² was computed for the slope model.

Table 2. Conditions of static compression using construction machinery

Weight of an excavator W	116 kN
Radius R	3.5 m
Acting load F	33.8 kN
Acting area through bucket A	0.9 m × 1.6 m
Pressure at compression p (F/A)	23 kN/m ²

This slope model was 3.0 m high, 4.0 m wide, 2.8 m long at the top and had a 45 degree inclination (Figure 5 and Figure 7a). Plastic sheets were placed to lubricate the surface between the soil and the concrete walls in order to reduce the friction.

Extensometers (DTP), inclinometers (ASG), and MPSMs were installed on the flat surface at the top of the slope prior to beginning the excavation (Figure 5c, Figure 6 and Table 3). Two sets of DTPs were installed along the line R10, as shown on Figure 7b, at an interval of 0.8 m so that increments of the displacement (d) could be measured. The sensor units of the DTPs were fixed on a beam bridging over both sides of the concrete walls, while extended thread wires were connected to pegs on the top. Two sets of ASGs were also installed along the line R10, and the measures were made at the same height as the DTPs, so that increments of the inclination (i) could be measured at the surface. In addition, six sets of MPSMs were installed in pairs, along the lines CL, R05 and R15 (Figure 7b). MPSMs of each pair were placed at a 0.8 m distance, as done with the ASGs, so that increments of the interpreted shear strain (θ) could be measured.

The interpreted shear strain (θ) is defined as the ratio of the differential movement (s) to the effective length (L) of the MPSM (Figure 7a), as shown by Equation 2 (Tamate Hori, Mikuni, and Suemasa, 2013).

$$\theta(\%) = \frac{s}{L} \times 100 \quad (2)$$

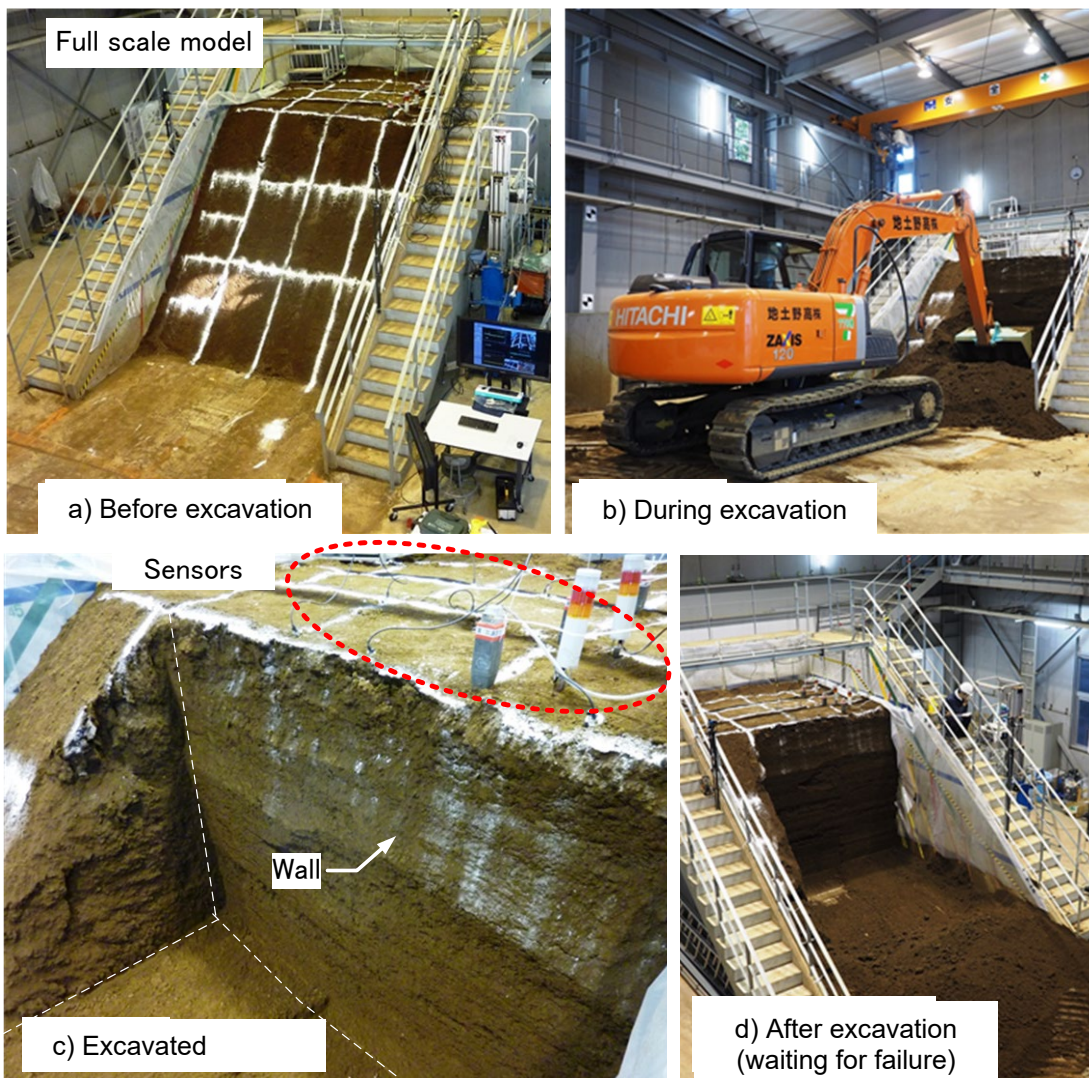


Figure 5. Progression of the excavation, which eventually caused instability of the slope.

Table 3. Sensor characteristics

Symbol	Type of sensor	Manufacture	Rated capacity	Rated output
MPSM	Bending beam-type transducers developed as Mini Pipe Strain Meter at JNIOSSH	MARUTO Testing Machine Co., Ltd	10.37 % (interpreted shear strain q)	3.0 mV/V
DTP	Wire-type Displacement Transducers (DTP-05MDS) used as extensometers	Kyowa Electronic Instruments Co., Ltd.	500 mm	5.0 mV/V
ASG	Accelerometers (AS-5TG) used as inclinometers		$\pm 49.03 \text{ m/s}^2 (\pm 5 \text{ G})$	0.5 mV/V

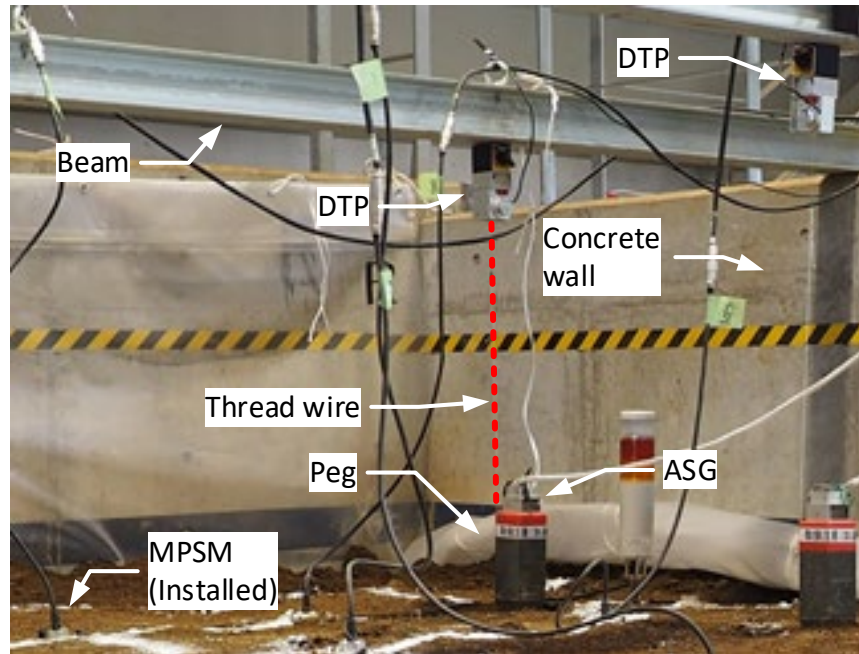
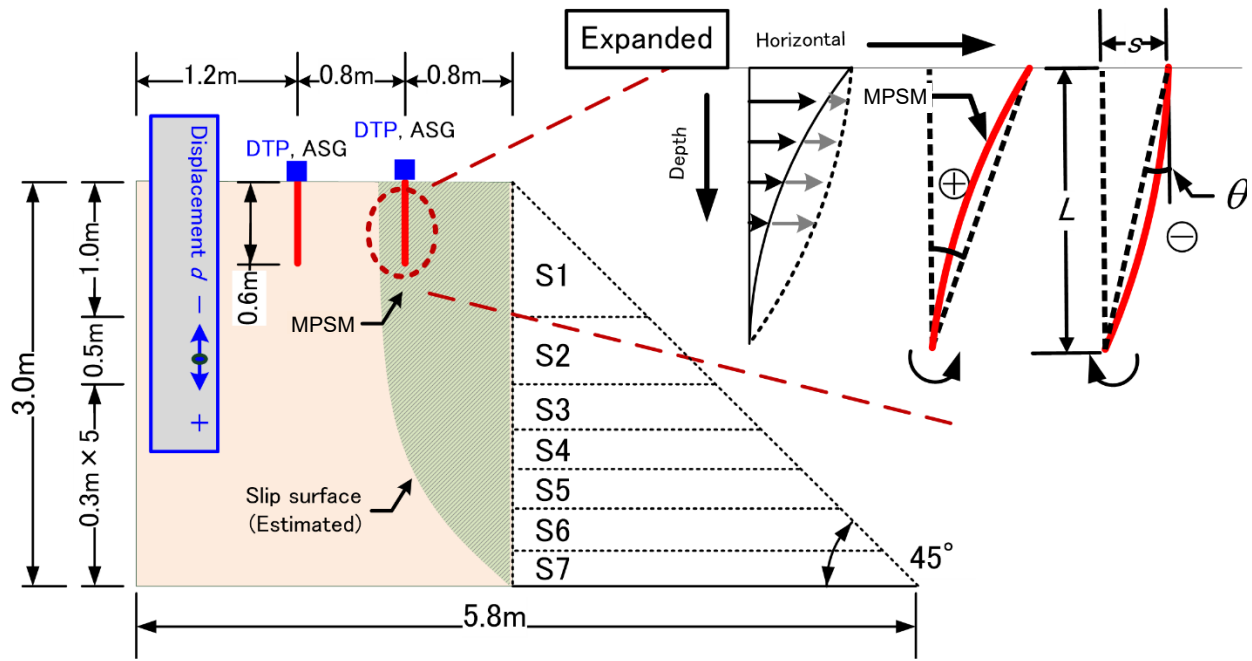


Figure 6. Installation of DTPs to measure surface settlement near the shoulder.

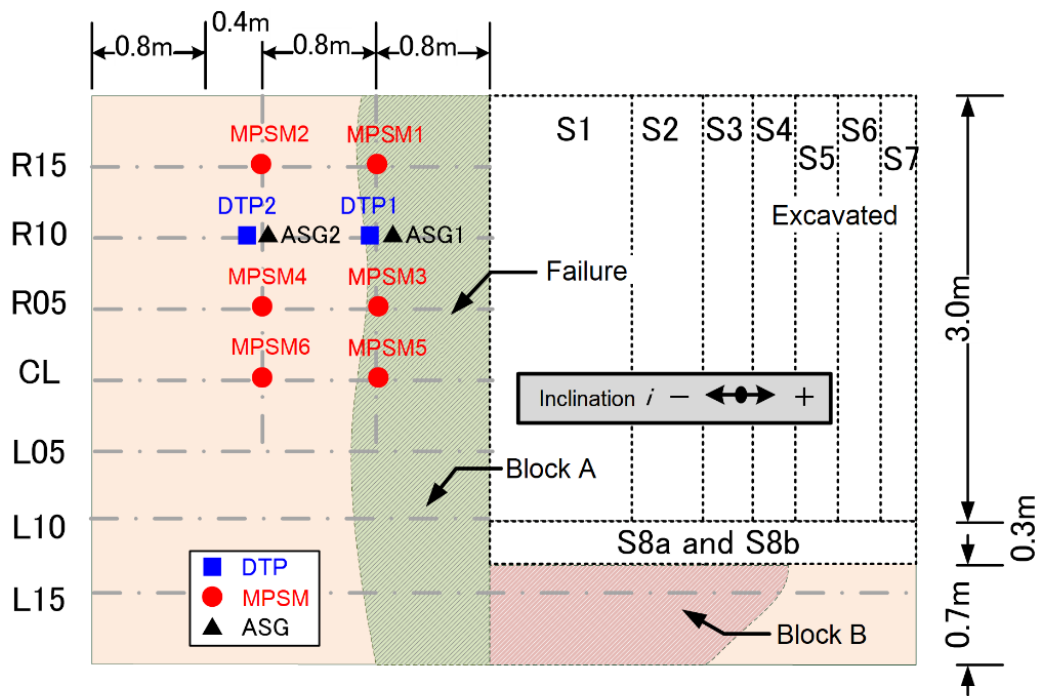
Eight steps of vertical excavation, from S1 to S8, were carried out by the excavator to make the slope unstable (Figure 7a,b). After step S7, as movements were not recorded by the sensors, steps S8a and S8b were added to the experimental plan. For steps S1 to S7, a 3.0 m wide excavation was made in the shoulder while step S8 consisted of excavating a 0.3 m wide strip along the left side of the slope model in two substeps (S8a with a width of 0.15 m and S8b with a width of 0.15 m, for a total width of 0.3 m). As indicated on Figure 10, the time interval between those two substeps was about 15 minutes.

A time interval of 30 minutes was allowed to observe any movement after excavation at each step (except between steps S5 and S6, where the time interval was about one hour, as seen on Figure 10). Each excavation bout lasted only a couple of minutes of the 30-minute interval.

Catastrophic failure occurred after 23 minutes from the final excavation during step S8b, performed at 3.0 m in depth.



(a) Profile view



(b) Plane view

Figure 7. Position of installed sensors and parts of excavation shown with (a) a profile view and (b) a plane view.

2.3.2 Experimental analysis of movement near the shoulder

Figure 8 shows the failure process of the excavated wall, illustrated by five pictures taken in about five seconds. Cracks at the top surface were opened up in Figure 8(a). The position of the failure block is also indicated in Figure 7b. Figure 8(b) and (c) show that a mass of soil fell down. The mass separated into smaller pieces (Figure 8(d)). Collapsed soil then spread over the floor (Figure 8(e)). As the remaining slope on the left side was still supporting the trench wall, the shoulder did not move in parallel at the beginning of the failure. However, the entire trench wall failed in the end.

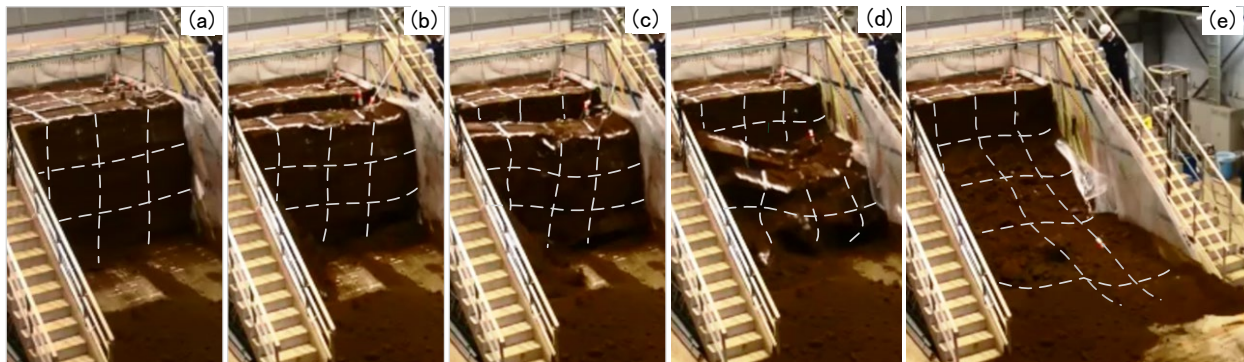


Figure 8. Process of failure of excavated wall in five seconds.

It was impossible for people to detect an increase in risk prior to failure by visual observation of the trench wall. This situation is dangerous as people who work in trenches are not aware of the increase in the threat indicated by the enlargement of the cracks (Tamate & Hori, 2018a). Figure 9 shows the shape of the trench after failure. Since the three curves R10, CL and L10 (see their location on Figure 7) are almost identical, the failure recorded in the lab is similar to plane strain conditions. A vertical wall appeared at an elevation between 1.6 and 3.0 m. The collapsed soil travelled a distance of about 5 m.

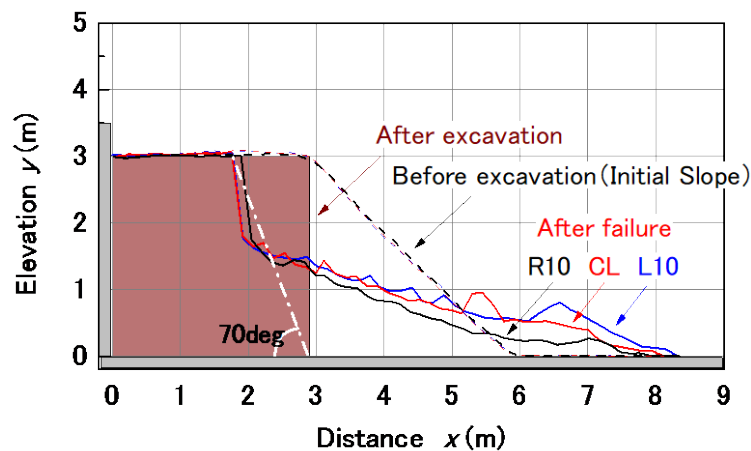


Figure 9. Profile shape of slope before and after excavation, and after failure.

Figure 10 shows the reaction from the three types of sensors – DTP, ASG and MPSM – from the beginning of the excavation until failure. The elapsed time T is shown on the lower horizontal axis. The excavation steps are labelled S1 to S8b on the upper horizontal axis. Fifteen-minute time intervals have been included to indicate a convergence of the increase between S8a and S8b. Two curves in each group of sensors show data that was obtained in two different rows. Experimental results were calculated under equivalent conditions with respect to distance from the shoulder. The excavated wall failed at 4.6 hours, when 23 minutes had passed after S8b of the final excavation step.

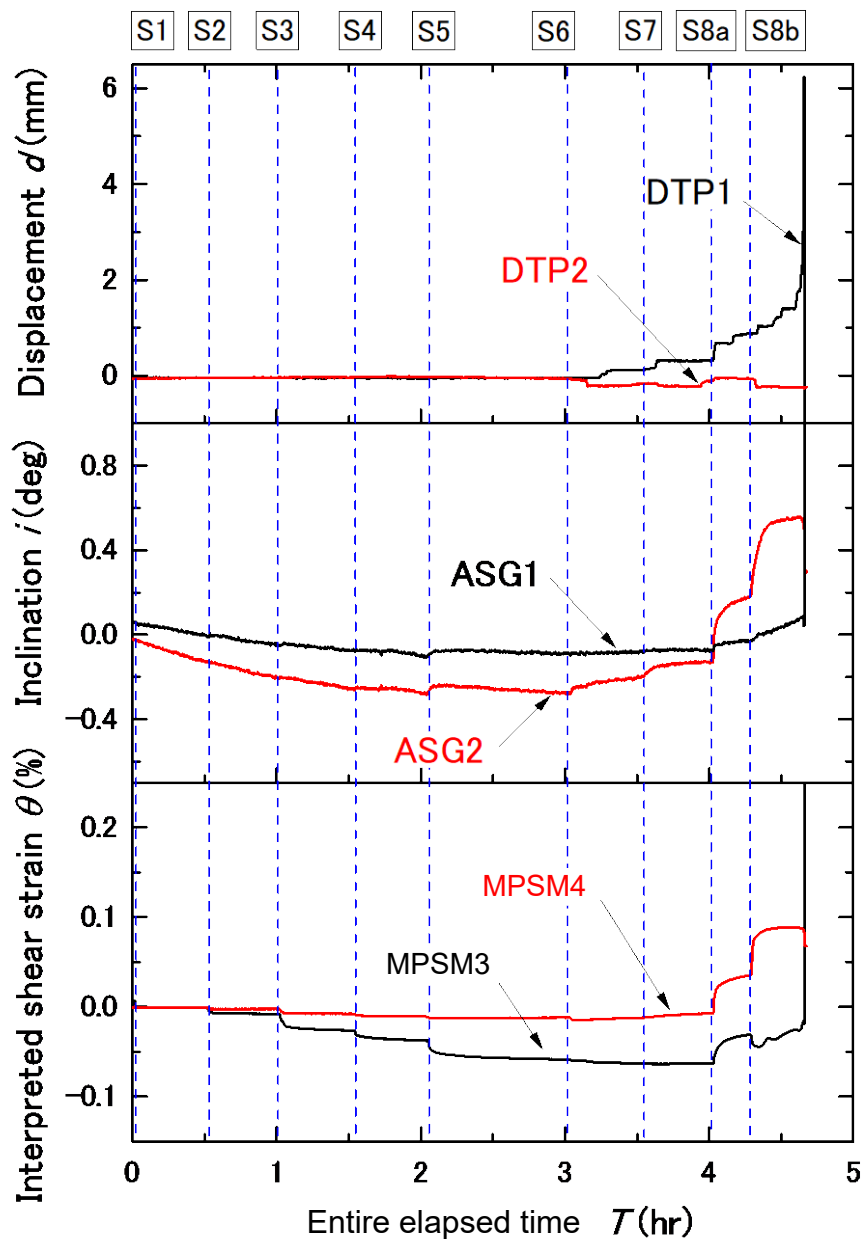


Figure 10. Reaction of DTP, ASG and MPSM sensors prior to failure.

An increase in the sensor reaction appeared prior to failure. The value of displacement d on sensor DTP1, which was located 0.8 m away from the shoulder, showed a clear increase after excavation S6. Moreover, the value increased significantly just a couple of minutes before failure. Meanwhile, DTP2 was positioned outside of the failure area (at 1.6 m from the shoulder) and its data did not show a clear increase.

The inclination signal i showed a slow decrease from the beginning of excavation S1. The decrease in ASG2, which was located further away from the shoulder, was greater than that of ASG1. Later on, these two ASG signals started increasing shortly after excavation S6. ASG2 data showed a two-step increment prior to failure while ASG1 showed a quick and large increase at failure following a gradual increase. For the ASG sensors, a larger reaction was recorded for the sensor positioned farther from the shoulder. Therefore, DTP and ASG data show opposite results in the relationship between the magnitude of the reaction and the distance from the shoulder. This could be because the direction of the reactions, which are either vertical or horizontal, are recorded differently by the sensors.

The MPSM3 and MPSM4 curves increased after S8a following a decrease between 0 and 4 hr. The shapes of the ASG and MPSM curves were quite similar (two-step shape). In addition, the amplitude of the increase for MPSM3 was almost 0.1% of θ , which was similar to MPSM4. It seems that placing the MPSM sensor a little farther from the shoulder (MPSM4 was positioned at a distance of 1.6 m from the shoulder) ensures a clearer reading of ground movement.

A decrease in the value θ of a MPSM (or an increase in a negative reading) means that a horizontal displacement has a barrel-shaped distribution with an increase in excavated depth. A positive increase means a horizontal strain that has a bow-shaped distribution. After S8b, the curves of DTP1, ASG1 and MPSM3 showed a linear increase prior to failure, though an acting load in the model was already constant when the final excavation S8b was completed. Accordingly, creep phenomena were detected in the measurements around the trench shoulder.

2.3.3 Discussion

2.3.3.1 Detection of potential threat of failure by identifying creep phenomena

The distribution of the horizontal strain in Figure 1 shows the existence of horizontal shear strain in the shallow subsurface. The MPSM reacts to ground movement with its bending deformation.

In 1965, Saito (1965) presented a study aiming to forecast the time of occurrence of a slope failure by identifying a second creep and a third creep from data records of displacement from extensometers. Fukuzono (1985, 1996) also proposed a method for predicting the failure time using the relation between an elapsed time (t_e) and the inversed value of the displacement rate ($1/v_d$). Failure occurs when a value of $1/v_d$ converges to zero. Therefore, a remaining time to failure can be estimated from a regression curve between t_e and $1/v_d$. The tested slope model revealed that creep phenomena exist in the form of shear strain in the shallow subsurface as well as does displacement on the surface of the slope.

Indeed, a clear increase in shear strain in the shallow subsurface was confirmed by the MPSM in the full-scale slope model. In addition, it was proven that this phenomenon reflects an increase in

potential threat of slope failure. Therefore, identifying either the second or the third creep could provide a couple of minutes for the workers to escape.

The left side of Figure 11 shows the relationship between the inverse of the shear strain rate $1/v_\theta$ and the remaining time prior to failure t_r on a logarithmic scale on the vertical axis. In this figure, v_θ is defined as the per-minute value of the increment of θ . Zero value for t_r corresponds to the trench failure time. Negative values of t_r indicate the remaining time prior to the failure. It can therefore be regarded as a type of velocity. When t_r was -10 , the $1/v_\theta$ values of MPSM1 were distributed at over 1000 min/%. This means that less than 0.001%/min of v_θ appeared 10 min before failure. However, $1/v_\theta$ shows a drastic decrease, whereas v_θ increased, when t_r went from -10 to 0 min.

The right side of Figure 11 provides an expanded view according to a linear scale on the right side vertical axis, showing $1/v_\theta$ values between 10 and 400 min/% when t_r was between -5 and -1 min. The values of v_θ were calculated as being between 0.0025 and 0.1 %/min. Consequently, in the same manner as for the second creep, the shear strain mostly accelerated in its increase. Accordingly, a clear increase in shear strain in the shallow subsurface was confirmed in the full-scale test model. In addition, it was proven that this phenomenon reflects an increase in potential threat of trench failure. Therefore, detecting creep phenomena would provide workers with a couple of minutes to escape.

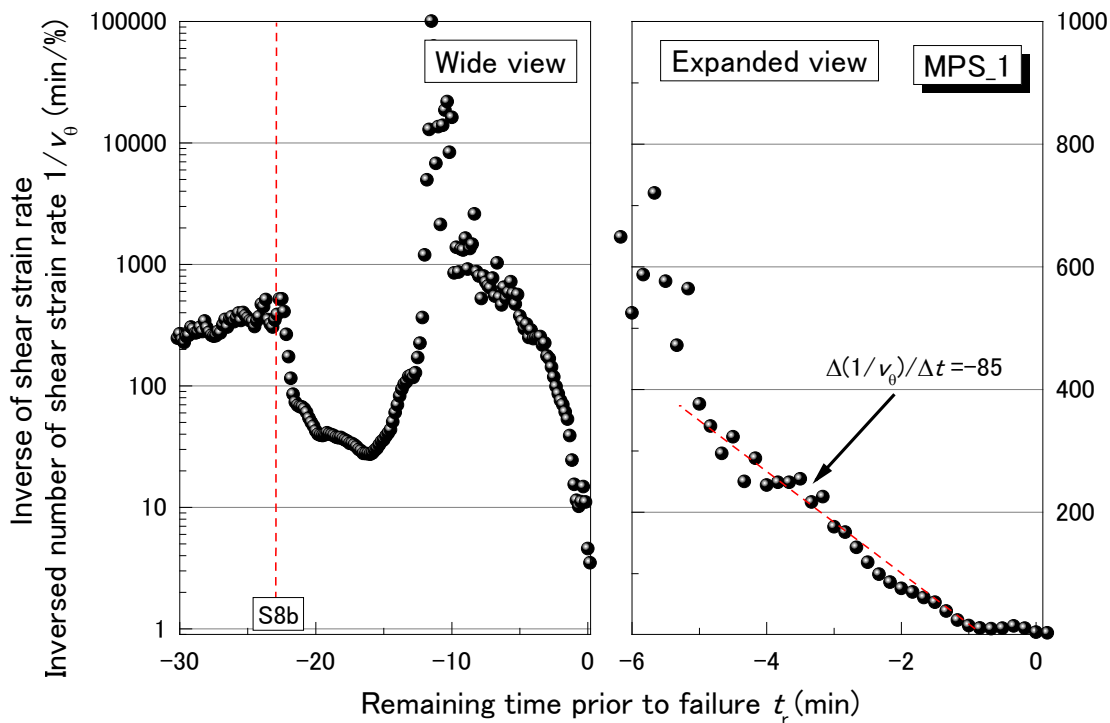


Figure 11. Inverse of velocity of shear strain as provided by MPSM1.

2.4 Conclusions of laboratory experiment

Tests with the full-scale slope model were carried out to assess the method of detection for the risk of trench failure during excavation. It was confirmed that both conventional sensors and the MPSM detected the threat of failure earlier than visual observation by an experimenter alone. As small movements were recorded by the sensors prior to failure, monitoring of this kind can detect threats.

Inclinometers and extensometers are widely used as conventional devices for monitoring landslides, which are generally large slope failures. These systems are composed of many sets of sensors, acquisition devices, electrical communications equipment, etc. In addition, significant time and expense are required to install these systems on site. Soil collapse monitoring for landslides contrasts sharply with that for trench failures, as the conditions of measurement for both time and area are quite different. In particular, the size of the area to be monitored is limited in small construction, such as excavation for trench and slope work. A couple of weeks are required for installing the necessary monitoring devices for large slopes that present a landslide risk. With such a long installation time, conventional sensors are not suitable for monitoring small excavations and slopes for workers safety; another system that is easy to install and to operate is needed.

The method that uses an MPSM has the advantage of simplicity and reactivity and can assist human observations on construction sites. Shear strain increases in the shallow subsurface as well as in the slip surface prior to collapse. It was determined that a couple of minutes could be provided for escape by detecting either the second or third creep. Accordingly, this laboratory experiment concludes that the threat of injury from collapsing soil can be reduced by using the proposed method and sensor (Tamate, Satoshi and Hori, 2017).

In summary, full-scale model tests of slope and wall failure in the laboratory (National Institute of Occupational Health and Safety, Japan [JNIOOSH], 2012), in Japan, showed that:

- 1) The MPSM detected the risk of slope failure for the specific conditions of the tests ;
- 2) Small shear deformations at shallow depths were clearly mobilized, which corresponded to the development of sliding surfaces in deeper parts;
- 3) Detection of the second or third creep could give workers a few minutes to evacuate the trench;
- 4) When the risk of slope failure or wall cave-in increased, it was not perceptible by observation alone;
- 5) No visible cracks were observed during the tests and no ground movement was visible before the failure;
- 6) The length of time before failure depended on the soil and on the specific conditions of the excavation;
- 7) The cave-in of the slope or wall could be predicted by measurement; therefore, the risk was also detectable by monitoring.

By warning that a collapse is imminent, the MPSM helps to reduce the risk of injury from cave-in. In short, the MPSM is not a method of preventing slope or wall cave-in, but rather a method of monitoring risks. Other safety measures should also be used in conjunction with the MPSM.

3. OBJECTIVE

The MPSM has been developed to monitor trench stability and wall collapse in typical soils of Japan, and laboratory test results showed the MPSM performed effectively with these soils. Therefore, the objective of the current expertise was to determine whether the MPSM would perform effectively *in situ* in sensitive clay, typical of the Champlain Sea, which makes up the subsurface of more than 80% of the inhabited territory of Quebec (Lafleur, Chiasson, Asselin & Ducharme, 1987; Lafleur, Silvestri, Asselin & Soulié, 1988; Péloquin, 1992).

As part of a collaboration between the JNIOH and the IRSST, the Mini Pipe Strain Meter, developed by JNIOH researchers, was used in the vertical wall of an unsupported excavation, during field tests carried out as part of a large research project entitled *Classification des sols et sélection des systèmes d'étalement pour l'excavation des tranchées* (Galy, LeBoeuf, Chaallal, & Lan, 2021, Report No. [R-1144-fr](#)). It was used to monitor the behaviour of the wall of the trench and to determine its ability to warn workers in time of imminent wall collapse so they can evacuate the excavation.

4. METHODOLOGY

4.1 Louiseville test site

Based on the results of a laboratory-testing program for intact clay samples of the Champlain Sea clay deposit (Lafleur, Chiasson, Asselin, & Ducharme, 1987; Lafleur, Silvestri, Asselin, & Soulié, 1988; Péloquin, 1992) carried out in 2017, the Louiseville site of the Quebec Ministry of Transport, Sustainable Mobility and Transport Electrification (MTMDET) was selected as the test site. This site is situated about 100 km northeast of Montreal (Figure 12).



Figure 12. Location of the municipality of Louiseville in relation to the Champlain Sea (Mer de Champlain) and the Laflamme Sea (Golfe de Laflamme).

Adapted from « Mer de Champlain », 2012 (retrieved June 20, 2020, https://fr.wikipedia.org/wiki/Mer_de_Champlain#/media/Fichier:Champlain_Sea.png)

Table 4 shows the geotechnical properties of the Louiseville test site (Demers & Leroueil, 2002; Leroueil et al., 2003), which are : water content (w), plasticity index (I_p), liquidity index (I_L), sensitivity (S_t), portion of particles with a diameter inferior to $2\ \mu\text{m}$, effective friction angle for the normally consolidated soil ($\Phi'_{n.c.}$), overconsolidation ratio (O.C.R.) and preconsolidation pressure (σ'_p).

Table 4. Geotechnical properties of Louiseville soils for a 200 mm sample

w (%)	I_p (%)	I_L (%)	S_t	< 2 μm (%)	$\Phi'_{n.c.}$ (°)	O.C.R.	σ'_p (kPa)
55–88	42	09–1.6	1.1–1.6	73–85	28	1.7–5.4	82–280

Figure 13 shows the undrained shear strength (S_u) and the residual undrained shear strength (S_{ur}) of the MTMDET's Louisville site, as measured by the IRSST and Laval University in 2018, and compared to the values obtained by Leroueil et al. (2003). Undrained shear strength values were obtained with either the shear vane test or the cone penetration test (CPT).

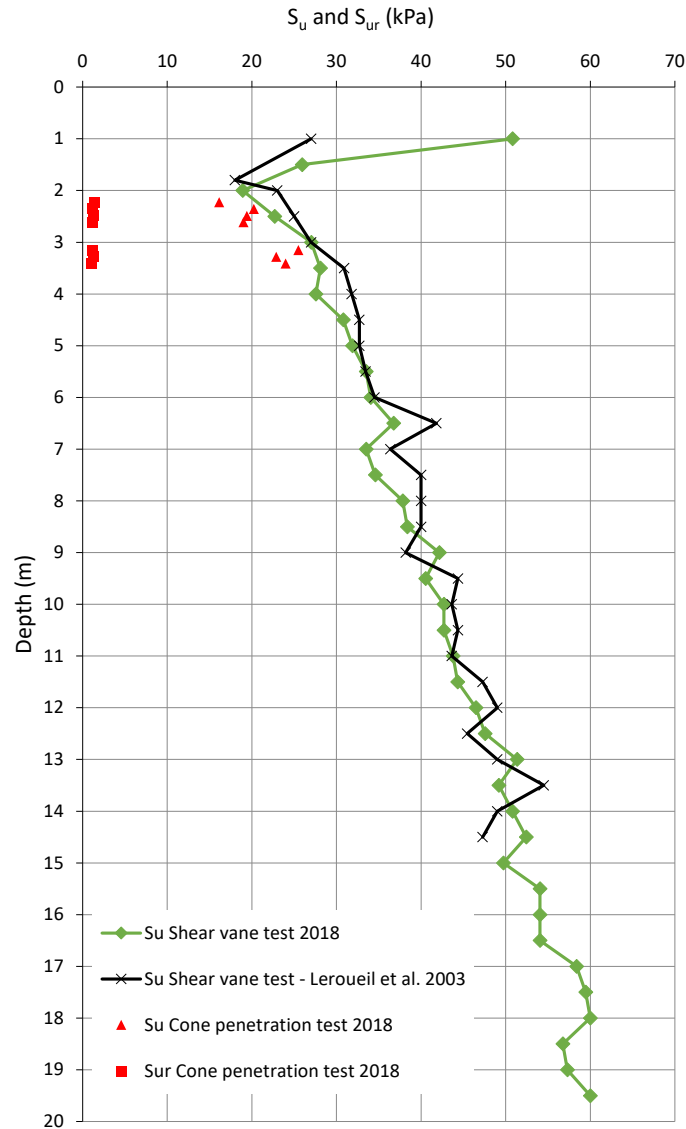


Figure 13. Undrained shear strength (S_u) and residual undrained shear strength (S_{ur}) of Louisville clay.

4.2 Experimental field tests

Experimental field tests were conducted within two of the trenches prepared for the IRSSST research project dealing with soil classification and selection of trenching shoring systems (Galy et al., 2021). Trenches A1 and A2, shown in Figure 14, were dug in sensitive clay soil at the Louiseville test site. A surcharge (q) of 30 kPa was applied by means of concrete blocks installed near the walls of A2 (Table 5).

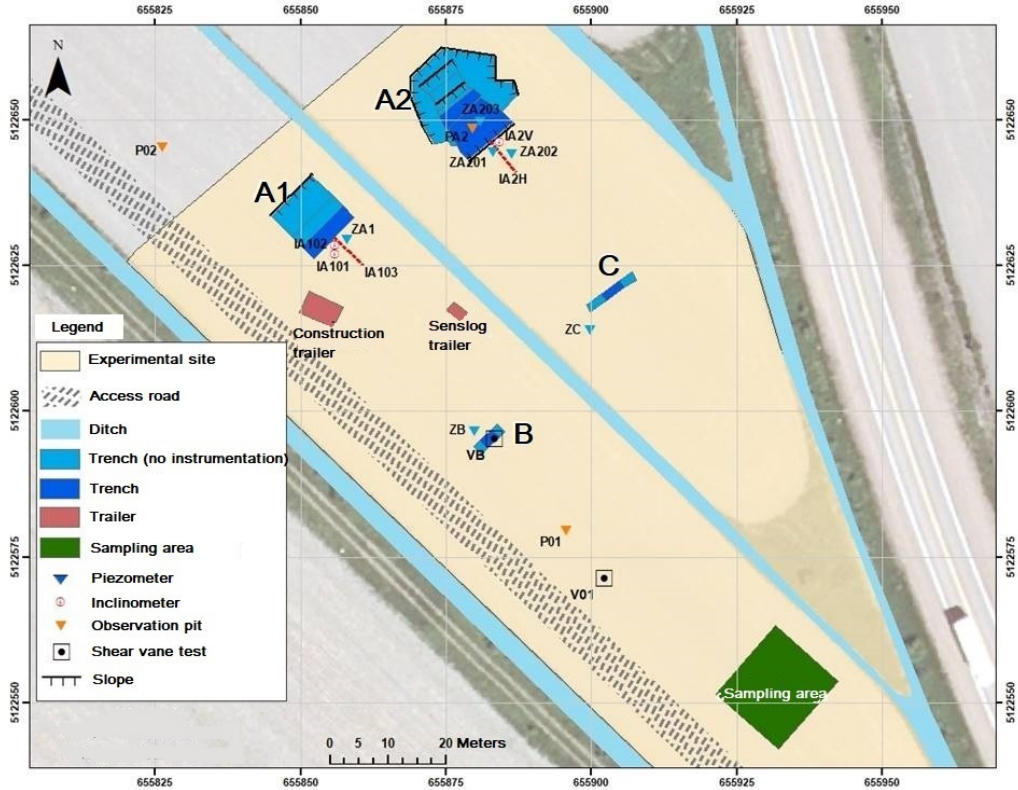


Figure 14. Trench layout.






Table 5. Experimental tests characteristics for sensitive clay soil

Series	Length (m)	Test section	Test n°	Description	Height H (m)	Surcharge q (kPa)
A	10	1	A1	Unsupported, 1 vertical wall and 1 benched wall	5	0
		1	A2	Unsupported, 1 wall at 1.6:1 slope and 1 benched wall	4.2	0
		1	A2	Unsupported, 1 wall at 1.6:1 slope and 1 benched wall	4.2	30

4.3 Site layout and instrumentation

Figure 14 shows the trench layout and the instrumentation used by the IRSST at the test site. The test site instrumentation is listed in Table 6 while details about the location of the different instruments used for trenches A1 and A2 are given in Figures 15, 16 and 18.

Table 6. Test site instrumentation and geotechnical tests

Instrument/test	Number	Description	Symbol
Piezometer	6	Roctest vibrating wire piezometers, PWL and PWS models (PWL model: 0.070 MPa capacity ; PWS model: 0.2 MPa capacity);	
Inclinometer	5	Measurand SAAV, 5 m length, subdivided in ten 500 mm sections, installed in 70 mm Geo-Lok tubes	
Tube samples	4	Laval University sampler (ϕ 200 mm, 600 mm height) (Rochelle, Sarrailh, Tavenas, Roy & Leroueil, 1981)	
Water table observation pit	3	1.8 m depth, open standpipe	
Shear vane test	2	Roctest M-1000	
Exploration pit	1	Realized in June 2017	
MPSM	4	1 autonomous MPSM 3 computer logged MPSM	

The SENSLOG system used for data logging was prepared by the Roctest Company. In his dissertation, Dourlet (2019) detailed the instrument calibration, installation and the data logging used for the project. He also described the procedures which were followed for the shear vane tests and tube sampling, as well as the observations made during the excavation of the exploration pit in June 2017.

4.3.1 Trench A1

Trench A1 was 10 m long, 8.75 m wide and 5 m deep, with 1 vertical wall and 1 benched wall, instrumented with piezometers, inclinometers and MPSMs, as illustrated in Figure 15. The *Safety Code for the construction industry* mentions that a mean of protection is mandatory for workers when a trench or excavation is deeper than 1.2 m. For the purpose of the current expertise, the 5 m depth was chosen in order to make sure that a failure of the trench wall would occur during our experiments. However, it should be noted that this would be highly unsafe working conditions and that this situation was a hypothetical scenario in order to assess the ability of the MPSM to predict wall failure through the estimation of the creep phenomenon.

Excavation of trench A1 began on May 8, 2018 with a Caterpillar 315D excavator. Before the excavation started, a grid pattern was drawn with white paint on the ground, adjacent to the vertical wall, for monitoring ground movement (Figure 16). Three MPSMs were installed at 1 m center-to-center spacing, with the first MPSM located at about 1 m from the vertical wall and connected to the alarm device (computer logged MPSM on Figure 15). An additional MPSM warning system was also installed at 1 m from the shoulder (autonomous MPSM on Figure 15).

This location was selected because an increase of shear strain prior to failure was measured in the shallow depth near the shoulder during the previous tests conducted at the JNIO SH laboratory. This location is convenient for real *in situ* use, as the available area where sensors can be installed is usually limited in urban excavation sites.

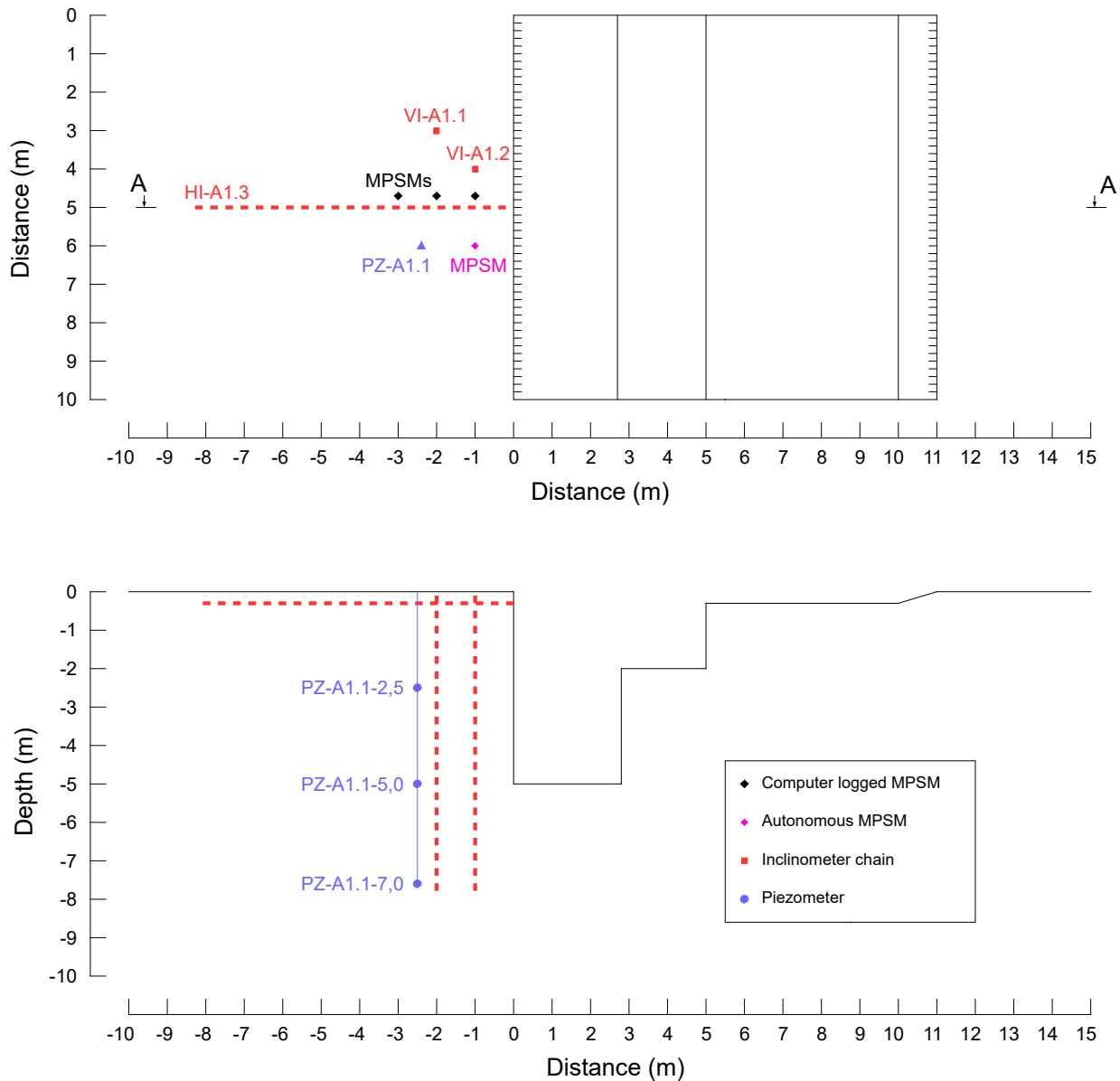


Figure 15. Plane view (top) and profile view (bottom) of trench A1, 10 m long, 8.75 m wide and 5 m deep, with 1 vertical wall and 1 benched wall.



Figure 16. Excavation of trench A1.

Specific excavation procedures were followed for trench A1 to ensure safety (Figure 17). Although the initial planned depth was 6 m, when site conditions became unsafe at around 5 m, it was decided to stop excavating at that depth (5 m).

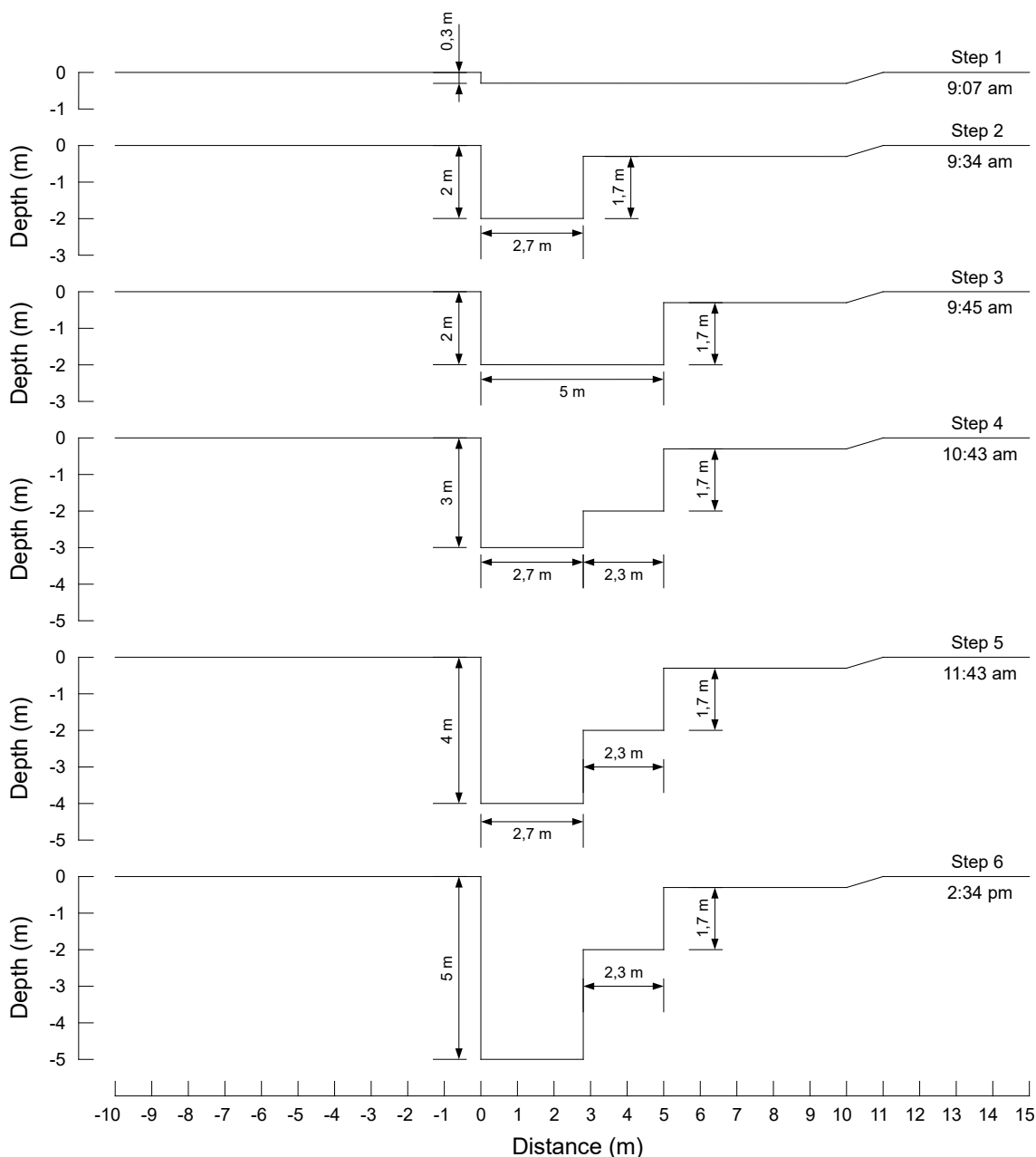


Figure 17. Excavation procedures for trench A1.

4.3.2 Trench A2

Trench A2 was 10 m long, about 20 m wide and about 4.2 m deep, with a 1.6:1 wall and a benched wall, and was instrumented with piezometers, inclinometers and MPSMs, as illustrated in Figure 18.

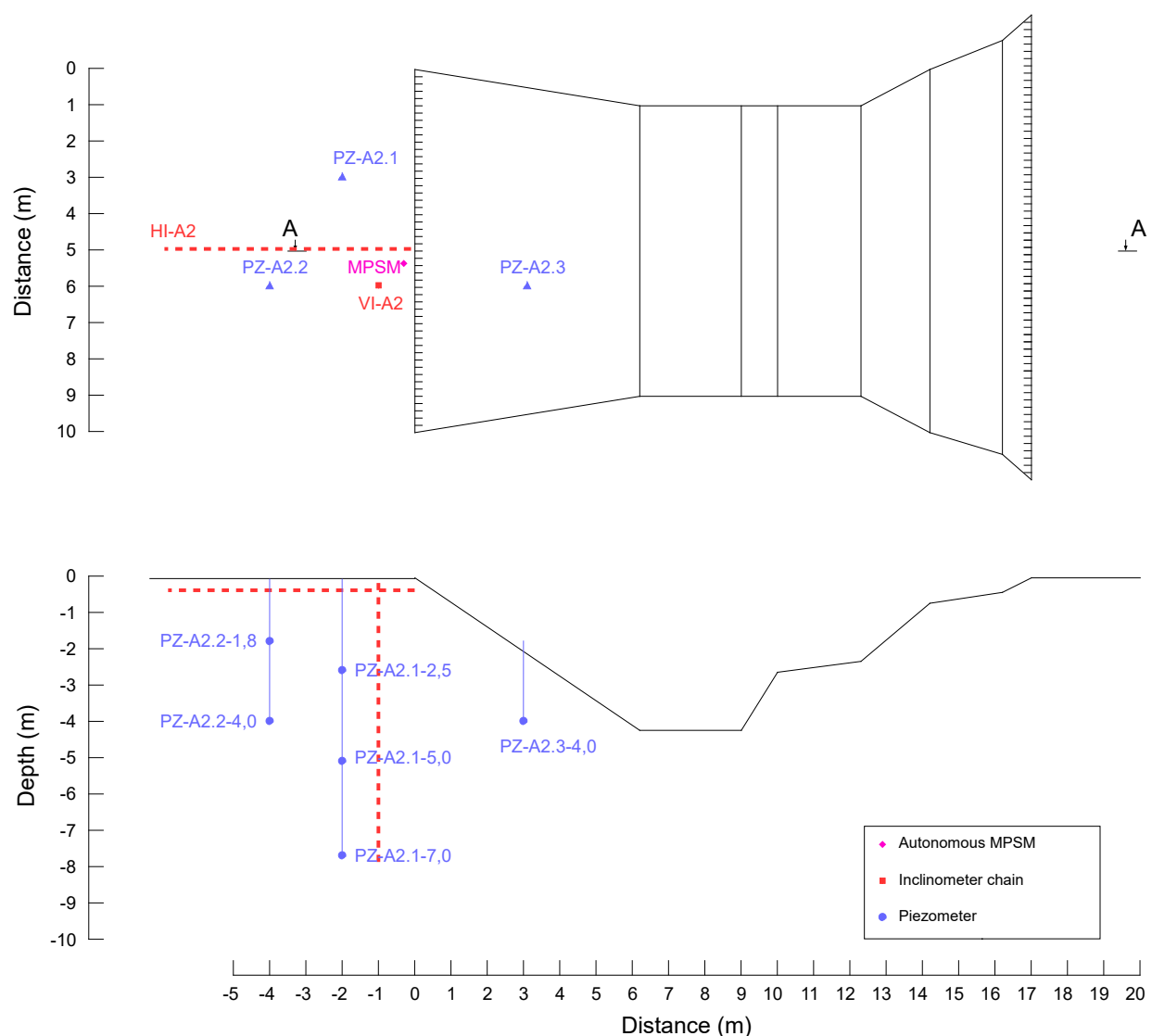


Figure 18. Plane view (top) and profile view (bottom) of trench A2, 10 m long, about 20 m wide and about 4.2 m deep, with a 1.6:1 wall and a benched wall.

4.3.2.1 Excavating trench A2

Before excavation began, a grid pattern was drawn with orange paint on the ground adjacent to the 1.6:1 wall, for monitoring ground movement (Figure 19). One MPSM was installed about 1 m from the 1.6:1 wall and was connected to the alarm unit, as shown in Figure 19. The digging was performed with a Caterpillar 315D excavator and a Caterpillar 320 excavator (Figure 20).

As for trench A1, specific excavation procedures were followed for trench A2, to ensure safety (Figure 21). The initial planned depth was 6 m, but when site conditions became unsafe at a depth of around 4 m, it was decided to stop the excavation at a depth of 4.2 m and to latter load the 1.6:1 wall with concrete blocks to simulate a 6 m deep wall. Figure 22 shows the progression of trench A2 as excavation was carried out.



Figure 19. Trench A2 with a rectangular pattern marked with orange paint to monitor ground movement.



Figure 20. Digging of trench A2 with Caterpillar 315 and Caterpillar 320 excavators.

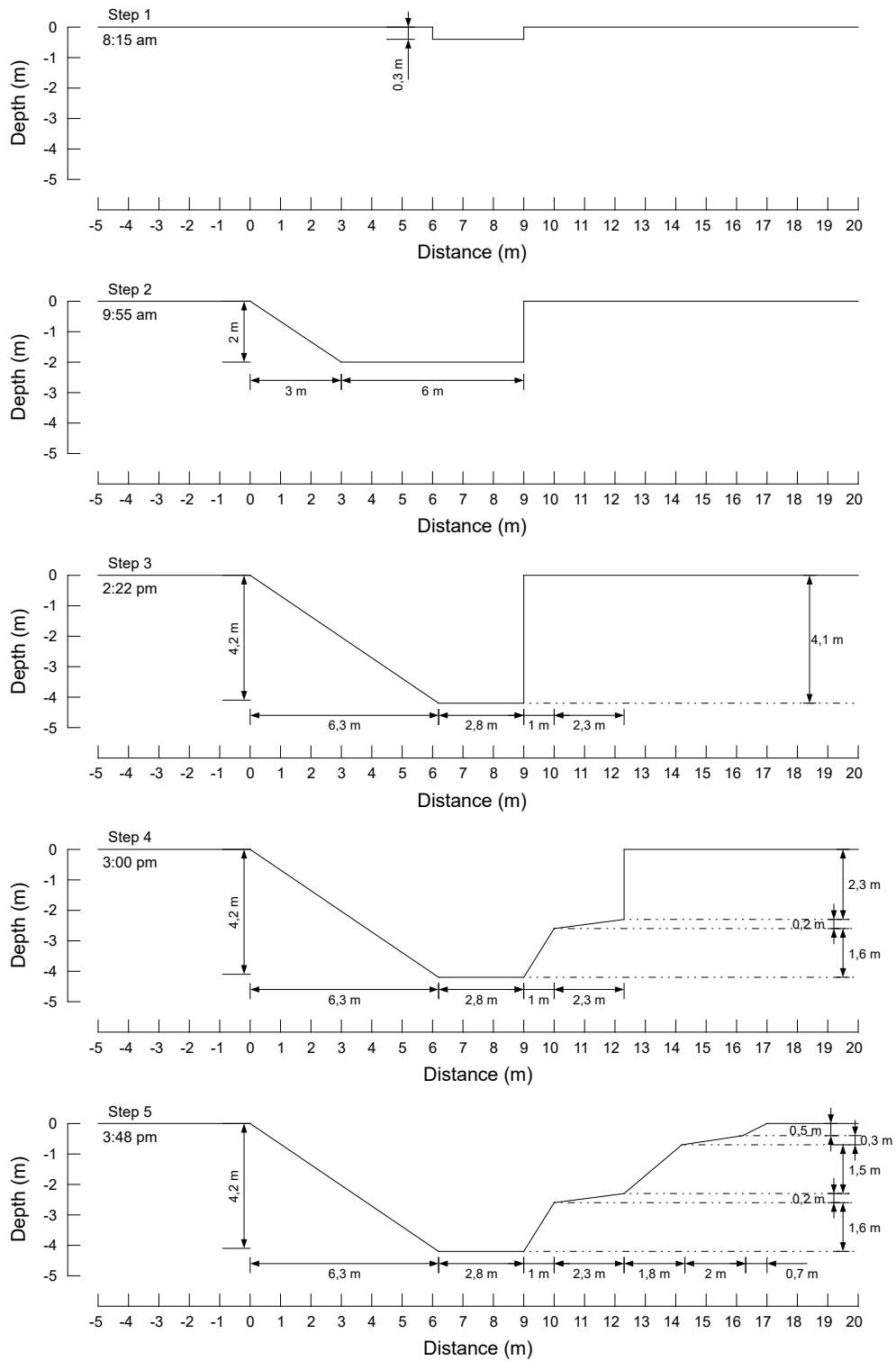


Figure 21. Excavation procedures for trench A2.




		
Step 2 Depth: 2 m 9:55 am	Step 3 Depth: 4.18 m 2:22 pm	Final Depth: 4.18 m 3:48 pm
Step by step excavation with 1.5:1 slope, with water infiltration in oxidized clay	Maximum depth for mechanical excavator used on site	Resulting trench A2

Figure 22. Progression of trench A2 as excavation was carried out.

4.3.2.2 Loading trench A2

Trench A2 was left open for three months. In order to simulate a 6 m deep wall, the 1.6:1 wall was loaded with concrete blocks and sand during the week of August 6, 2018. The 1.6:1 wall was initially loaded with concrete blocks (Figure 23) following a first (Figure 24) and a second (Figure 25) loading patterns.



Figure 23. Loading of trench A2 with concrete blocks.

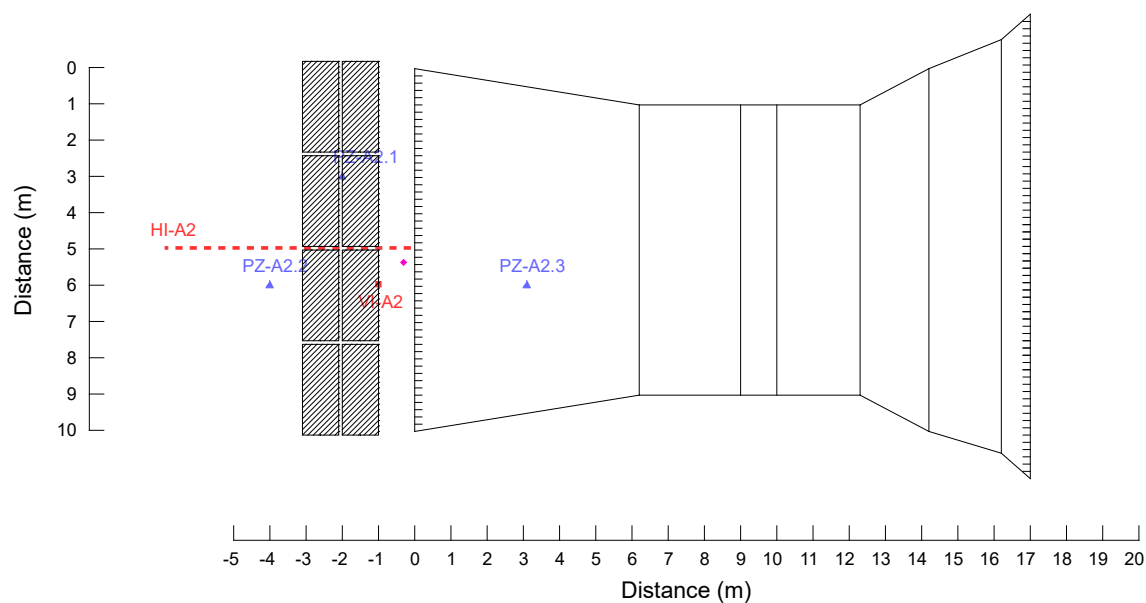


Figure 24. First loading pattern of trench A2 with concrete blocks.

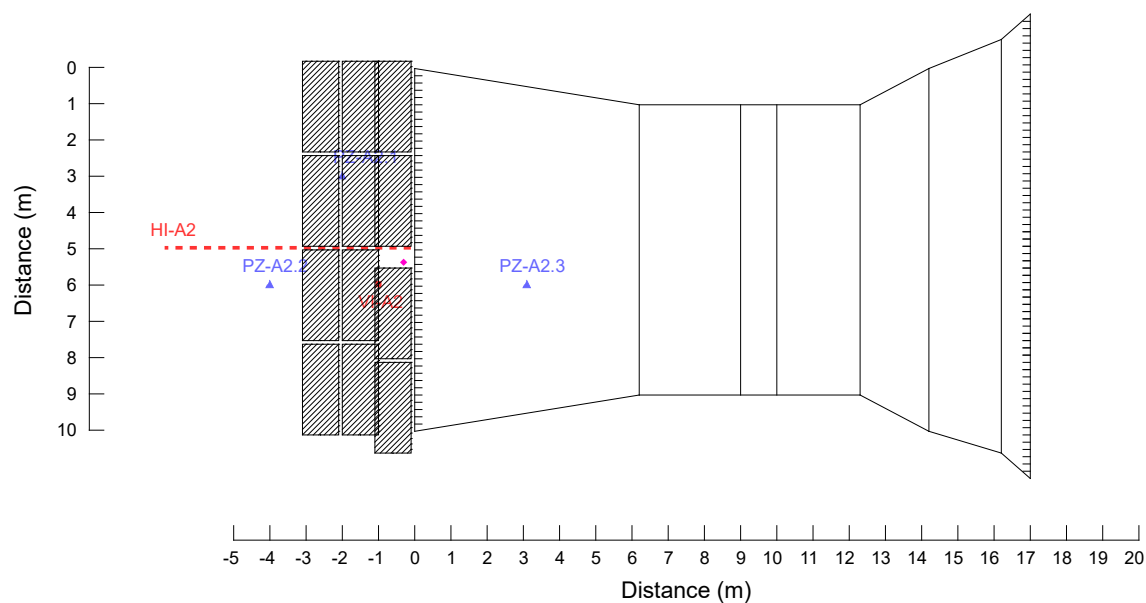


Figure 25. Second loading pattern of trench A2 with concrete blocks.

The surcharge for the 1.6:1 wall was then reaching approximately 30 kPa when sand was added next to the concrete blocks, as shown in Figure 26 and Figure 27.



Figure 26. Loading of trench A2 with concrete blocks and sand.

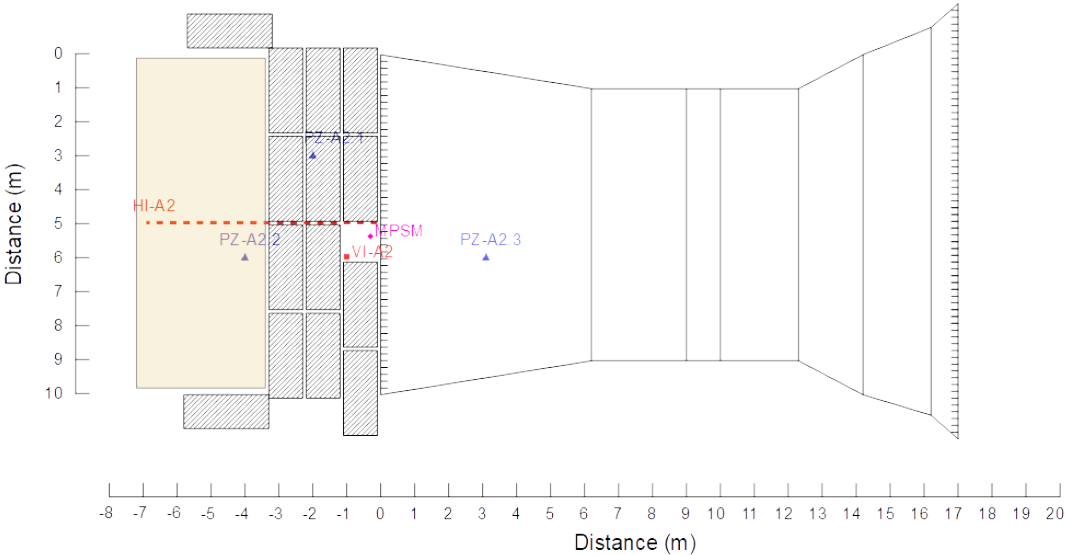


Figure 27. Additional loading of trench A2 with sand.

5. OBSERVATIONS AND RESULTS

5.1 Weather monitoring during tests

Table 7 presents the meteorological observations in Louiseville throughout the summer of 2018 and a comparison to the mean for the 1982–2012 period. When the trenches were excavated, the water table was very high, and the soil conditions at the time may have been detrimental to long-term trench stability. However, the summer was very dry in Louiseville in 2018 (Table 7), with only 171.3 mm of rain for the May–August period (usually 360 mm), and only 117.9 mm during the actual test period (May 8 to August 11). Not only was the summer dryer than usual, the temperatures were also higher: from 0.5 to 3.6°C higher than usual if the mean temperature for each month is considered. In particular, in 2018, warmer mornings and nights (+2.4 to +6°C) and slightly warmer afternoons (+0.3 to +1.2°C, with the exception of June which was -1.7°C) were recorded.

Table 7. Meteorological observations at Louiseville for summer of 2018

Observation period	1982–2012				2018*				Test period* (May 8 – August 11, 2018)			
	May	June	July	August	May	June	July	August	May	June	July	August
Mean temperature (°C)	12.0	17.4	20.2	18.7	13.6 (1.6)	17.9 (0.5)	22.8 (2.6)	22.3 (3.6)	14.1 (2.1)	17.9 (0.5)	22.8 (2.6)	23.8 (5.1)
Minimal mean temperature (°C)	5.7	11.3	14.1	12.7	8.1 (2.4)	14.0 (2.7)	18.9 (4.8)	18.7 (6)	8.6 (2.9)	14.0 (2.7)	18.9 (4.8)	20.8 (8.1)
Maximal mean temperature (°C)	18.4	23.5	26.3	24.7	19.0 (0.6)	21.8 (-1.7)	26.6 (0.3)	25.9 (1.2)	19.6 (1.2)	21.8 (-1.7)	26.6 (0.3)	26.7 (2)
Rain (mm)	79	91	93	97	39.2 (-39.8)	30.4 (-60.6)	67.5 (-25.5)	34.2 (-62.8)	15.3 (-63.7)	30.4 (-60.6)	67.5 (-25.5)	4.7 (-92.3)

* Numbers in parentheses are indicating differences from the values reported for the same month during the 1982-2012 period.

5.2 Trench A1

5.2.1 Observations and behaviour of trench A1 as excavation progressed – May 8, 2018

Excavation of trench A1 began on May 8, 2018, at around 9:00 a.m. At around 9:34 a.m. (approximately step 3 on Figure 17), at a depth of 2 m, a vertical rupture due to flaking and fragmentation of weathered brown clay and water inflows in the oxidized clay was observed (Figure 28).



Figure 28. Rupture due to flaking and water inflow during excavation of trench A1 (step 3).

The flashing yellow light of the MPSM came on to indicate detection of the second creep phenomenon of D1 around 12:06:15 (step 5), which lasted 22 minutes. At 12:27:18, the flashing red light of the MPSM came on to indicate detection of the third creep phenomenon, which lasted 22 seconds, and a large block of soil broke away, causing the wall to recede by 1 m. The JNIO SH alarm unit was carried away with debris to the bottom of the trench (Figure 29). The trench was left untouched for about 2 hours and step 6 began at 14:34.



Figure 29. Rupture of vertical wall at a depth of 5 m, carrying the MPSM to bottom of the trench.

At about 14:34, at a depth of 5 m, during the excavation of step 6, a large block of soil broke away, causing the wall to recede by 1.75 m, resulting in a total trench width of 9.75 m. The IA1-2 inclinometer was carried away in the cave-in (Figure 30). The JNIO SH alarm unit was retrieved

from the bottom of the trench prior to the excavation of step 6. As the trench stability was questionable, for safety reasons, the researchers did not proceed to the reinstallation of the MPMSM at the shoulder of the trench. Thus, it was not possible to assess the ability of the MPMSM to predict the trench collapse for step 6.

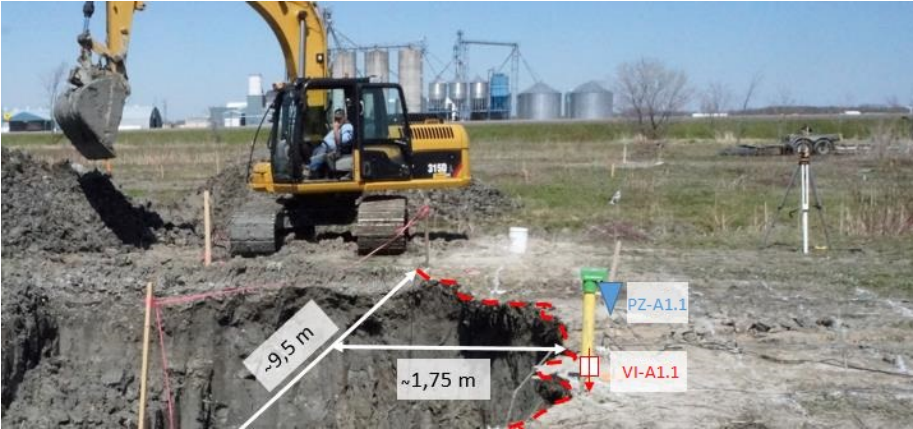


Figure 30. Major block of soil broke away, causing the wall to recede by 1.75 m.

5.2.2 Piezometer data

Figure 31 shows the piezometer results for the collapse of trench A1 on May 8, 2018.

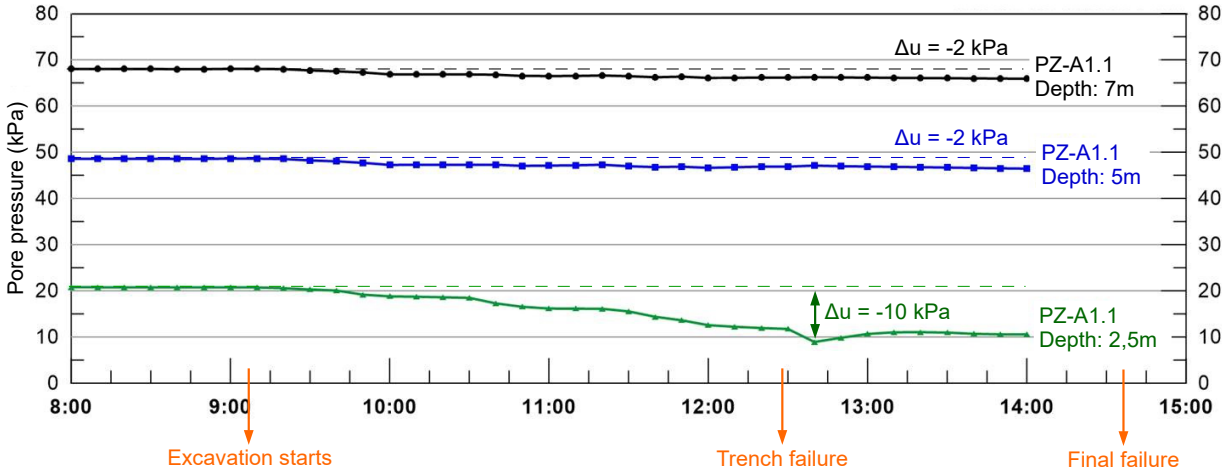


Figure 31. Piezometer results for trench A1, during excavation on May 8, 2018.

Piezometric data shows a notable reduction in pore pressure for the top piezometer (PZ-A1.1): -9 kPa when the vertical wall of the trench collapsed. However, the data does not show a clear acceleration in the decline of the pore pressure that could have helped to anticipate the vertical wall failure with precision.

5.2.3 Inclinator data

Figure 32, Figure 33 and Figure 34 show the results for the inclinometers VI-A1.1, VI-A1.2 (both vertical) and HI-A1.3 (horizontal) respectively. The two vertical inclinometers show a maximum horizontal displacement ΔX of 45 mm at the top for the closest inclinometer to the vertical wall of the trench (VI-A1.2) and of 23 mm at the top for the other one (VI-A1.1). The inclinometer tubes were protruding 0.5 m above the soil level, meaning that at a depth of 3.5 m, no noticeable horizontal displacement was measured by the instruments. The ΔY displacements were quite limited (around 5 mm), indicating that the vertical wall displacement was relatively symmetrical. The horizontal inclinometer measured a 20 mm vertical displacement of the soil.

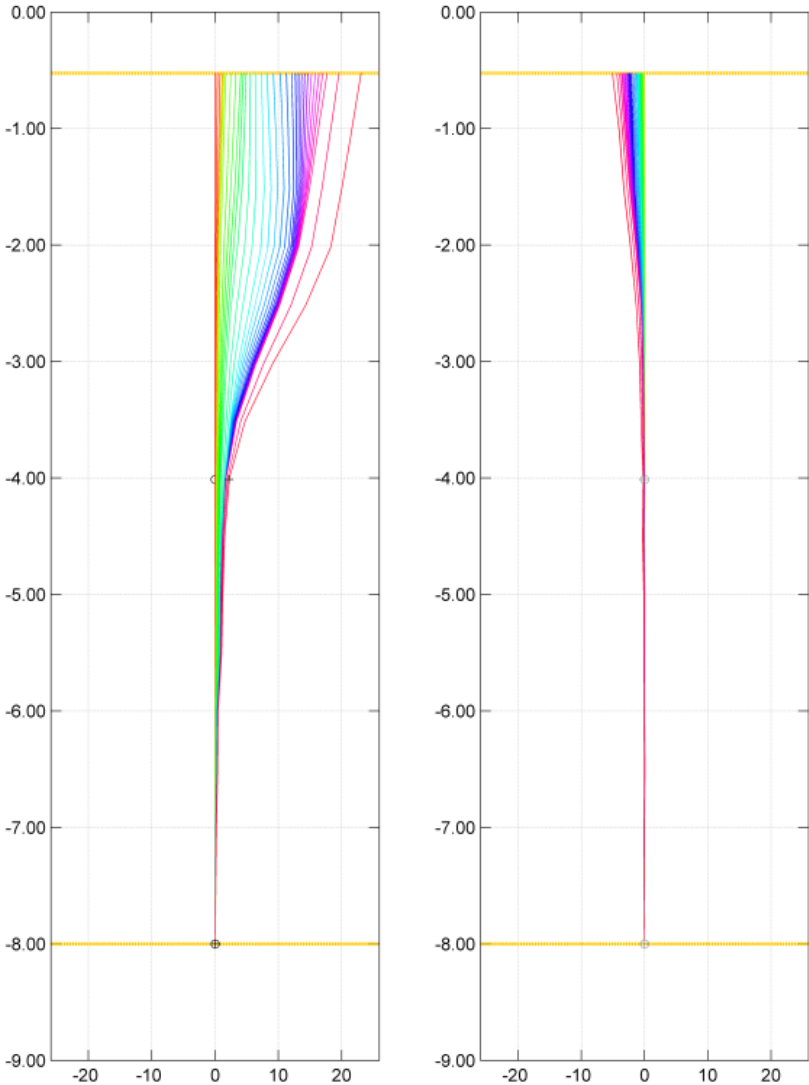


Figure 32. Vertical inclinometer VI-A1.1 (left = ΔX , right = ΔY , results in mm).

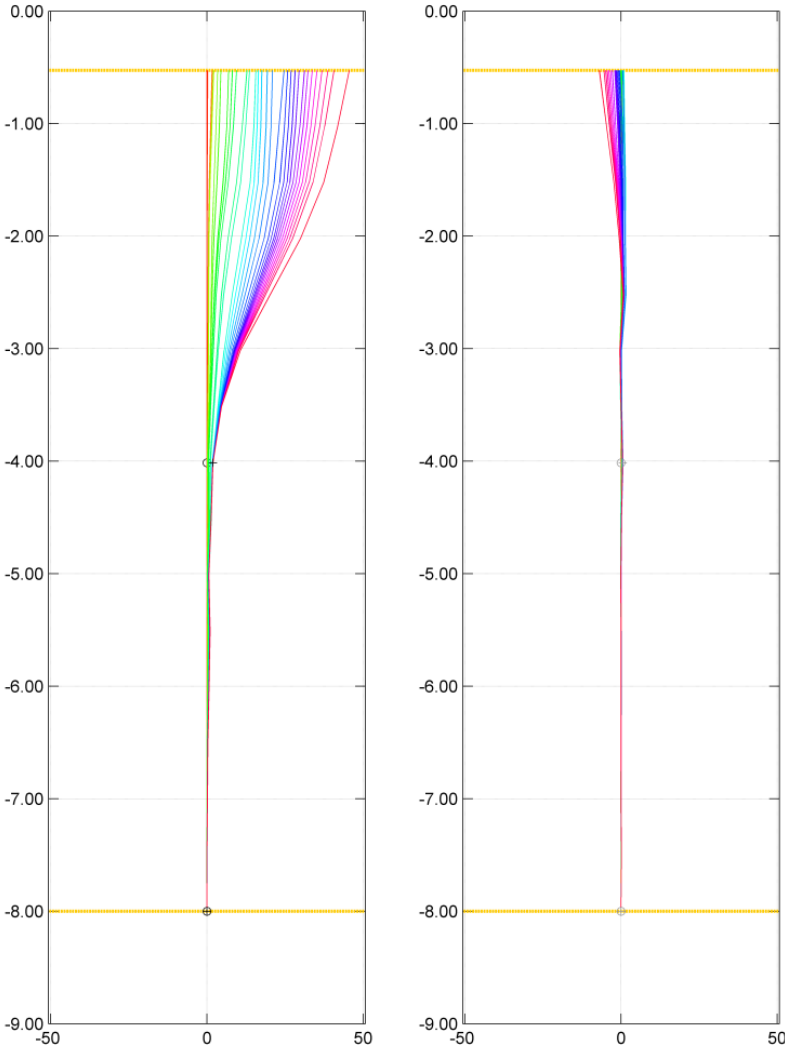


Figure 33. Vertical inclinometer VI-A1.2 (left = ΔX , right = ΔY , results in mm).

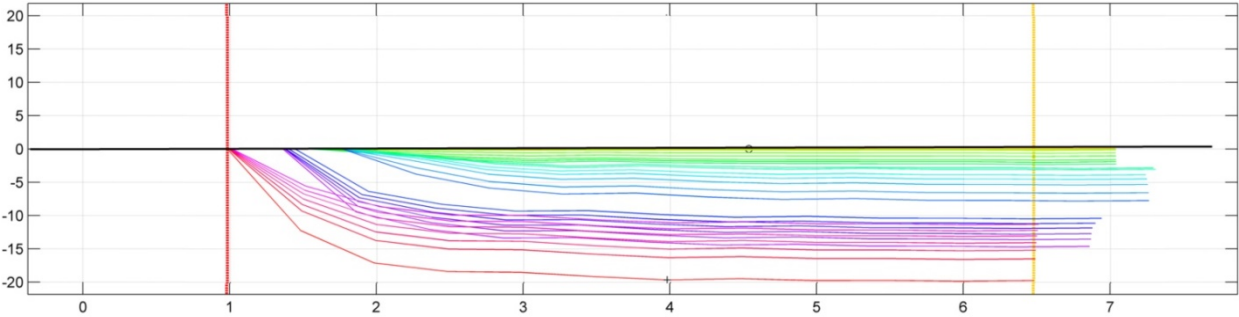


Figure 34. Horizontal inclinometer HI-A1.3 (results in mm).

5.2.4 MPSM data

Trench A1 failure occurred during unattended hours; it was recorded by the IRSST camera. The analysis of the photos taken by the camera shows the beginning of the observation of trench A1 until its failure detected by the MPSM. The pictures also helped us to see and understand whether the MPSM alert system functioned or not prior to failure.

Figure 35 shows the flashing yellow light of the D1 warning, following the detection of the second creep phenomenon, while Figure 36 shows the flashing red light of the D2 warning, following the detection of the third creep phenomenon.



Figure 35. Flashing yellow light of D1 warning, following the detection of the second creep phenomenon prior to failure.



Figure 36. Flashing red light of D2 warning, following the detection of the third creep phenomenon prior to failure.

The warning lights did indeed turn on prior to the failure, even though heavy sunshine made it difficult to see the flashing signals. The times at which the D1 and D2 warnings were triggered coincided perfectly with the photographic record and with the analytical results. The MPSM alert

system therefore functioned fully in the field test. D1 and D2 warnings were given prior to the failure when monitoring detected an increase in shear strain in the shallow subsurface near the shoulder of trench A1. Figure 35 and Figure 36 show good reaction to the ground movement. The MPSM measured an increase in the risk of trench failure as the excavation progressed.

5.3 Trench A2

Trench A2 remained open throughout the summer for a total of 92 days, with no visible signs of failure.

5.3.1 Piezometer data

Figure 37 shows the trench A2 piezometer results for the period from May 5 to August 11, 2018. The loading of the concrete blocks was done on August 6, 2018. As can be seen from the piezometer data, pore pressure declined throughout the summer, which suggests that the horizontal stress in the soil was gradually released as the summer progressed. It is worth noting that the water table was approximately 0.5 m below the soil surface in early May and around 2.5 m below the surface in August. As mentioned in Section 5.1, the summer of 2018 was warmer and dryer than usual. An increase in pore pressure was recorded on August 6, which corresponds to the 30 kPa load applied to the top of the trench.

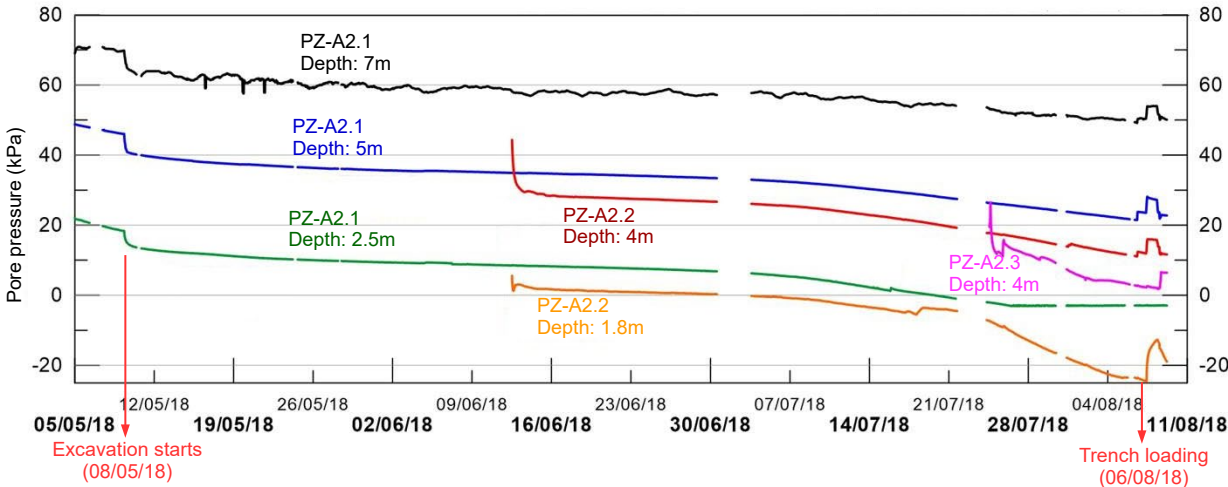


Figure 37. Results of the piezometers A2.1, A2.2 and A2.3 for the period from May 5 to August 11, 2018.

5.3.2 Inclinerometers results

Figure 38 shows the vertical inclinometer (VI-A2) results. The vertical inclinometer recorded a small horizontal displacement (7 mm) at the top of the trench, but almost no displacement at the bottom of the trench (depth of 4.2 m).

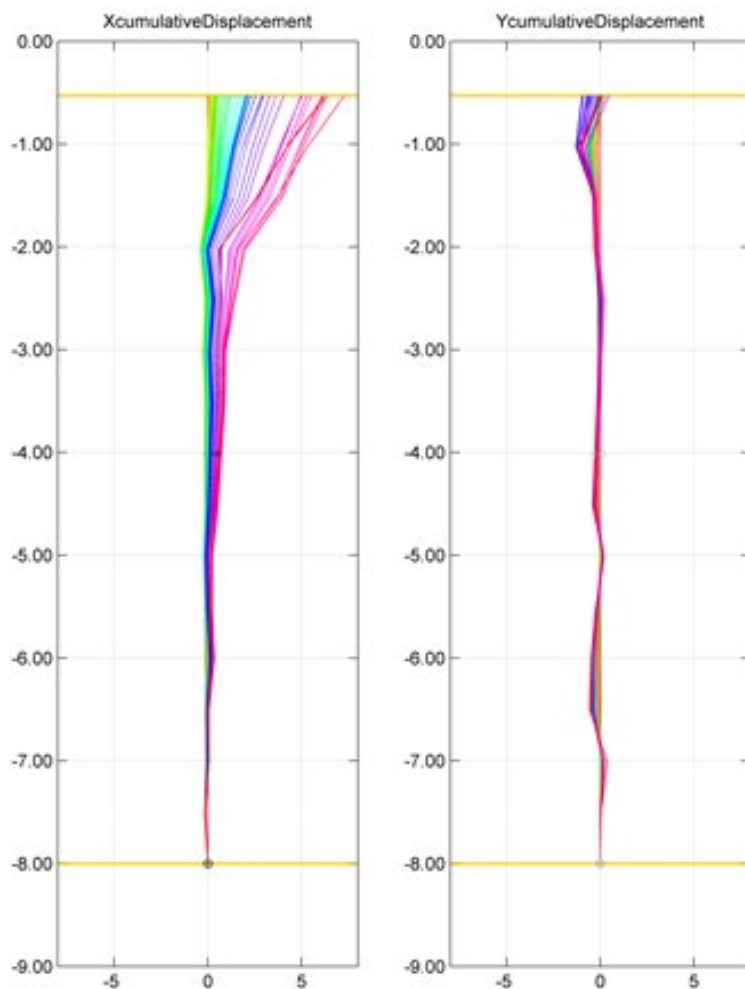


Figure 38. Vertical inclinometer results (VI-A2) for trench A2 (left = ΔX , right = ΔY , results in mm).

The horizontal inclinometer (HI-A2) recorded a maximum vertical displacement of 27 mm at a distance of 3.5 m from the top of the trench, which corresponds to the last row of concrete blocks installed on August 7 (Figure 39).

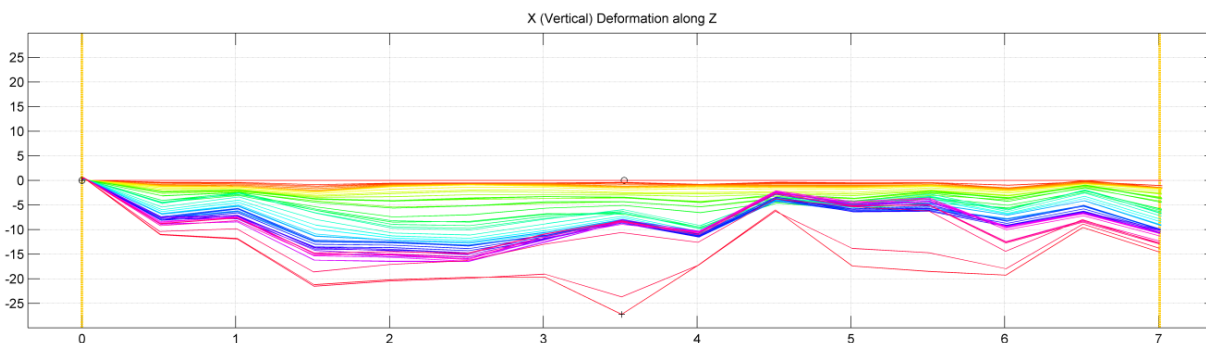


Figure 39. Horizontal inclinometer (HI-A2) results for trench A2 (results in mm).

5.3.3 MPSM data with loading of concrete blocks

The MPSM was installed at the top of the trench on August 6, at 10:42 a.m. (Day 1). The loading began at 2:15 p.m. on the same day. The recording was stopped on August 8 at 9:00 a.m., giving a total recorded time of approximately 46 hours (Figure 40). Notable events occurring throughout this recording period are listed in Table 8 for Day 1 and in Table 9 for Day 2.

As can be seen from Figure 40, a slight increase in shear strain was recorded shortly after the MPSM was installed in the ground, as the soil settled around the MPSM sensor. Then, at the beginning of the loading of the trench with concrete blocks, a clear increase in shear strain can be noted over approximately four hours after the installation of the MPSM. The device's alarm went off twice (Table 8), corresponding to the placement of blocks in close proximity to the MPSM sensor. Those two events are also observable in Figure 41, as well as in Figure 42, when the inverse of the shear strain rate ($|1/v_{\theta}|$) fell below 100 min/%.

After the initial loading on Day 1, the trench was left to settle for approximately 18 hours. A slight gradual increase followed by a slow decrease in interpreted shear strain can be seen during that period (Figure 40, shown between the two loading days).

Figure 43 shows the interpreted shear strain as a function of time, for the second loading of trench A2, on Day 2. First, a third row of concrete blocks was put in place, nearer to the edge of the trench. This loading did not have a clear effect on the interpreted shear strain. Once the third row of blocks was in place, sand was loaded at the back of the rows of blocks. A decrease in interpreted shear strain was initially recorded during loading, and when the soil deposit was left to settle, the interpreted shear strain increased again until 6:00 p.m. (18:00). Then the interpreted shear strain declined throughout the night and seemed to have stabilized by the morning (Figure 40, $t_e \approx 45$ hrs).

The loading of trench A2 with concrete blocks and sand, for a total pressure of 30 kPa, did not affect trench stability. Trench A2 was left open for 92 days in total, with no visible signs of failure that could be measured by our instruments. The reliability of the MPSM alarm system warning of imminent trench failure could therefore not be assessed in the case of trench A2, because no soil failure occurred.

Table 8. Timeline of notable events during loading of trench A2 with concrete blocks on Day 1 (August 6, 2018)









Time	Alarm	Event	Figure
14:15	-	Start of loading	 A yellow CAT excavator is shown in the process of lifting a concrete block. The site is an open field with some vegetation and a few workers in the background.
14:20:17	D1 and D2	Placing concrete blocks in close proximity (first row)	 The excavator is positioned over a row of concrete blocks, carefully placing them. Several workers are standing nearby, observing the process.
14:27:47	D1 and D2	Placing concrete blocks in close proximity (second stack of first row)	 The excavator is now placing a second stack of concrete blocks on top of the first row. The workers are still present, monitoring the operation.
14:58	-	End of loading on Day 1, two rows of concrete blocks (two stacks for each row)	 The final state of the trench area, showing two rows of concrete blocks, each with two stacks. Workers are gathered around the trench, and the excavator is no longer visible.

Table 9. Timeline of notable events during loading of trench A2 with concrete blocks on Day 2 (August 7, 2018)

Time	Event	Figure
9:25	Start of loading on Day 2, placing a third row of concrete blocks	
9:42	Placing the side blocks of concrete	
9:50	Loading with sand	
11:10	End of loading (rain started at around 10:15)	

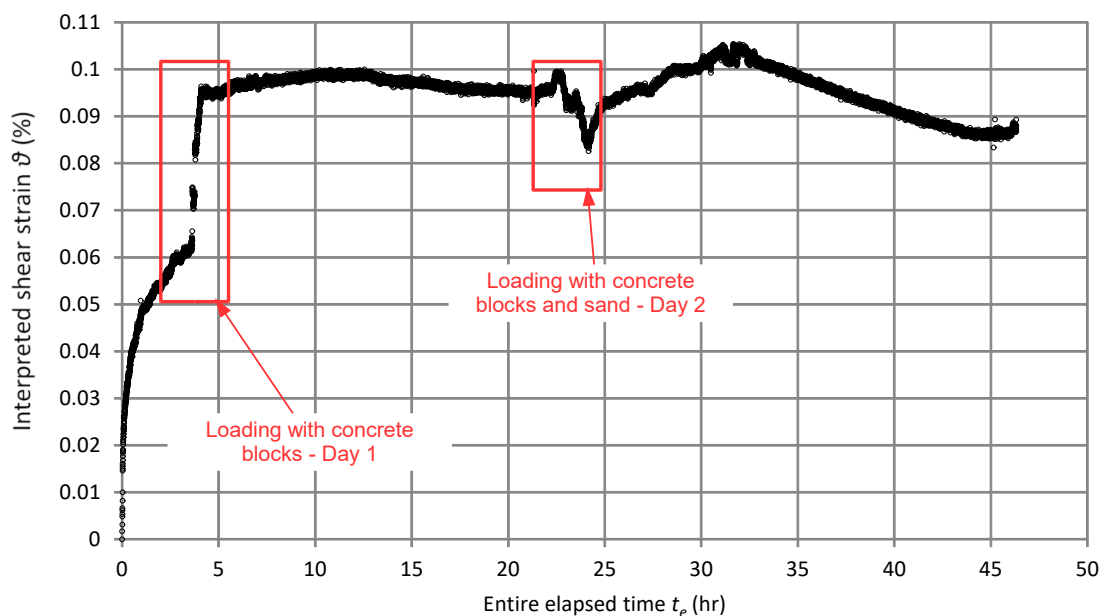


Figure 40. MPSM results during trench A2 loading, showing two specific loading periods (Day 1 and Day 2).

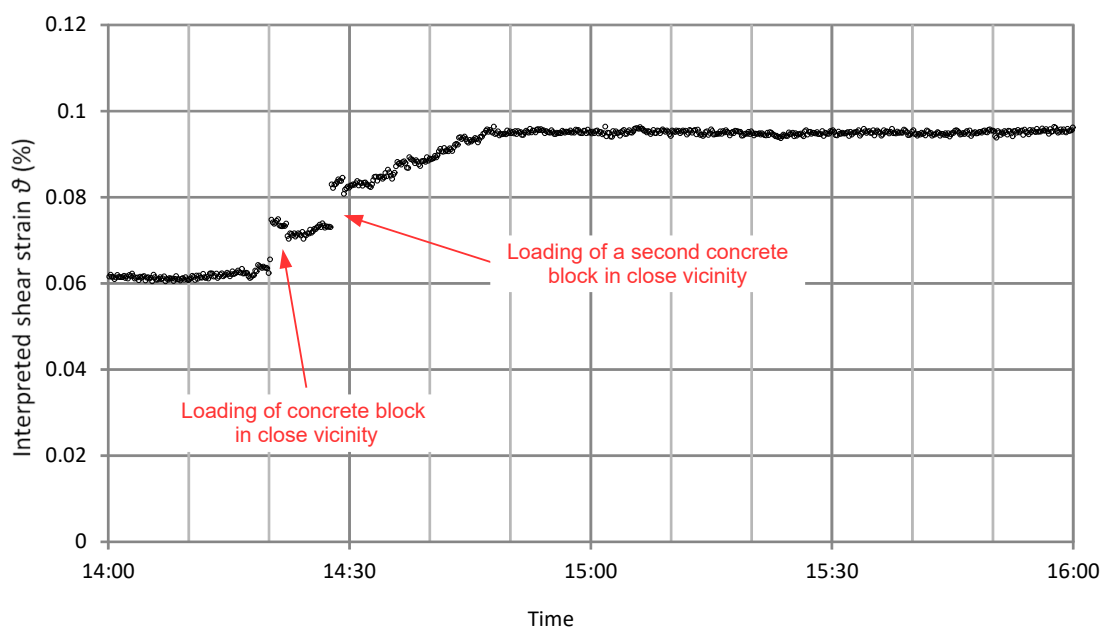


Figure 41. MPSM results during first loading of trench A2 with concrete blocks, showing the effect of placing blocks in the close vicinity of the device.

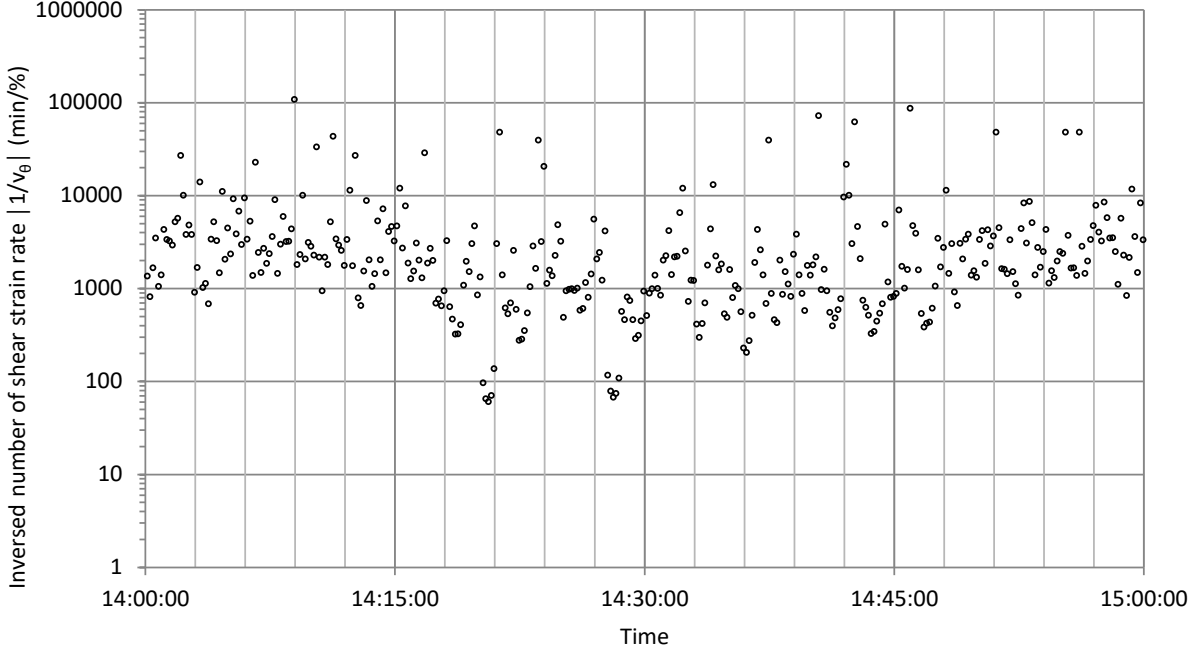


Figure 42. Inverse of shear strain rate $|1/v_{\theta}|$ as a function of time for trench A2 during the first loading with concrete blocks (Day 1).

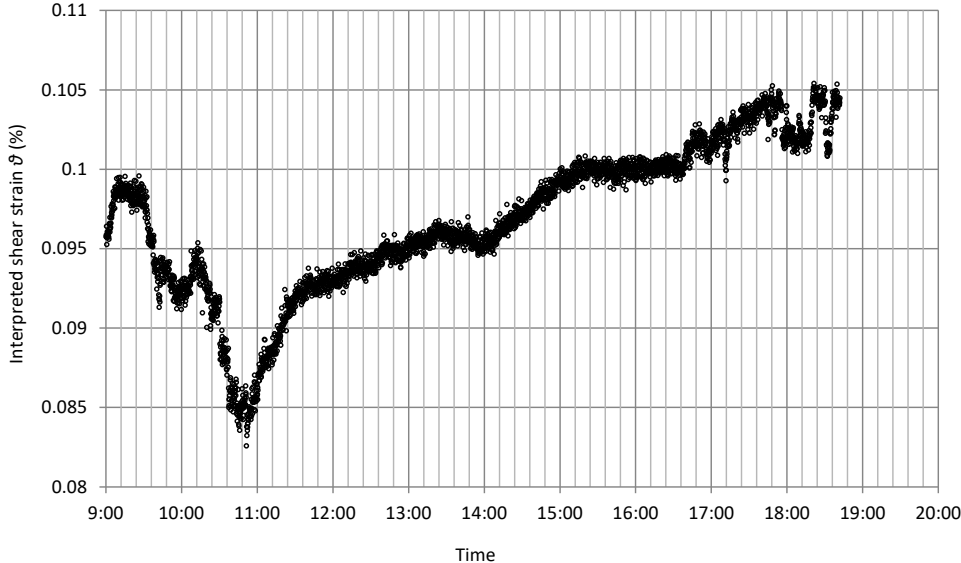


Figure 43. MPSM results during second loading of trench A2 with concrete blocks and sand.

6. ANALYSIS AND INTERPRETATION OF MPSM DATA FOR TRENCH A1

The analysis and the interpretation of the MPSM data are presented in this chapter. Figure 44 shows the relationship between the interpreted shear strain θ and the entire elapsed time (t_e) during the excavation of trench A1. Values of θ gradually increased over the course of the first excavation, as the depth increased from zero to 2 m. After the first excavation, the values of θ were almost constant between 0.84 and 1.43 hr of elapsed time t_e .

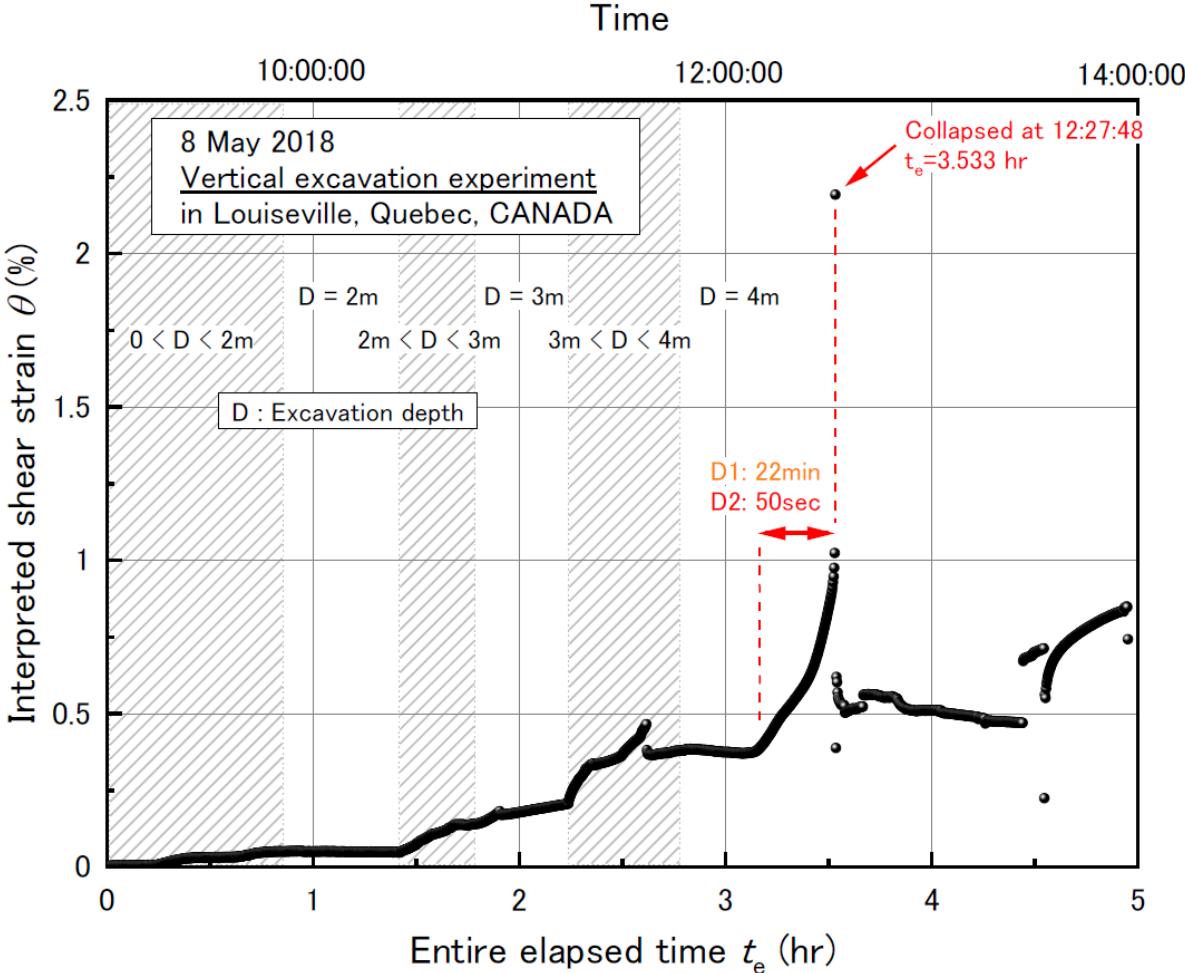


Figure 44. Relationship between interpreted shear strain θ and the entire elapsed time.

A large increase in θ appeared in the second excavation when the depth increased from 2 to 3 m. However, the values of θ mostly converged again after completion of the second excavation. The values of θ increased more in the third excavation than in the second one. The values of θ abruptly dropped at 2.63 hr of t_e so that the curve shows a discontinuous point. It seems that a small soil block dropped in the vertical cutting surface at that moment. The value of θ remained constant after this small failure.

However, the values of θ then began increasing again from 3.16 hr of t_e . The rate of increase was almost constant. After θ increased for about 20 minutes, the trench wall failed completely at 3.533 hr of t_e .

Figure 45 shows an expanded view of the relationship between θ and t_e prior to failure. The values of θ increased almost linearly between 3.16 and 3.44 of t_e , even though no excavation was carried out at that time (D remained constant at 4 m). This linear increase was therefore considered the result of the second creep. The MPSM alert system functioned and triggered a D1 warning of flashing yellow lights during this period. A tangent modulus of the curve is defined as a mean shear strain rate v_θ (%/min) that is an increment of θ per minute.

In addition, the increase in the value of θ gradually accelerated starting at 3.46 hr of t_e , as a third creep phenomenon appeared. The MPSM alert system estimated the appearance of the third creep at 50 seconds before failure, causing the D2 warning to be triggered.

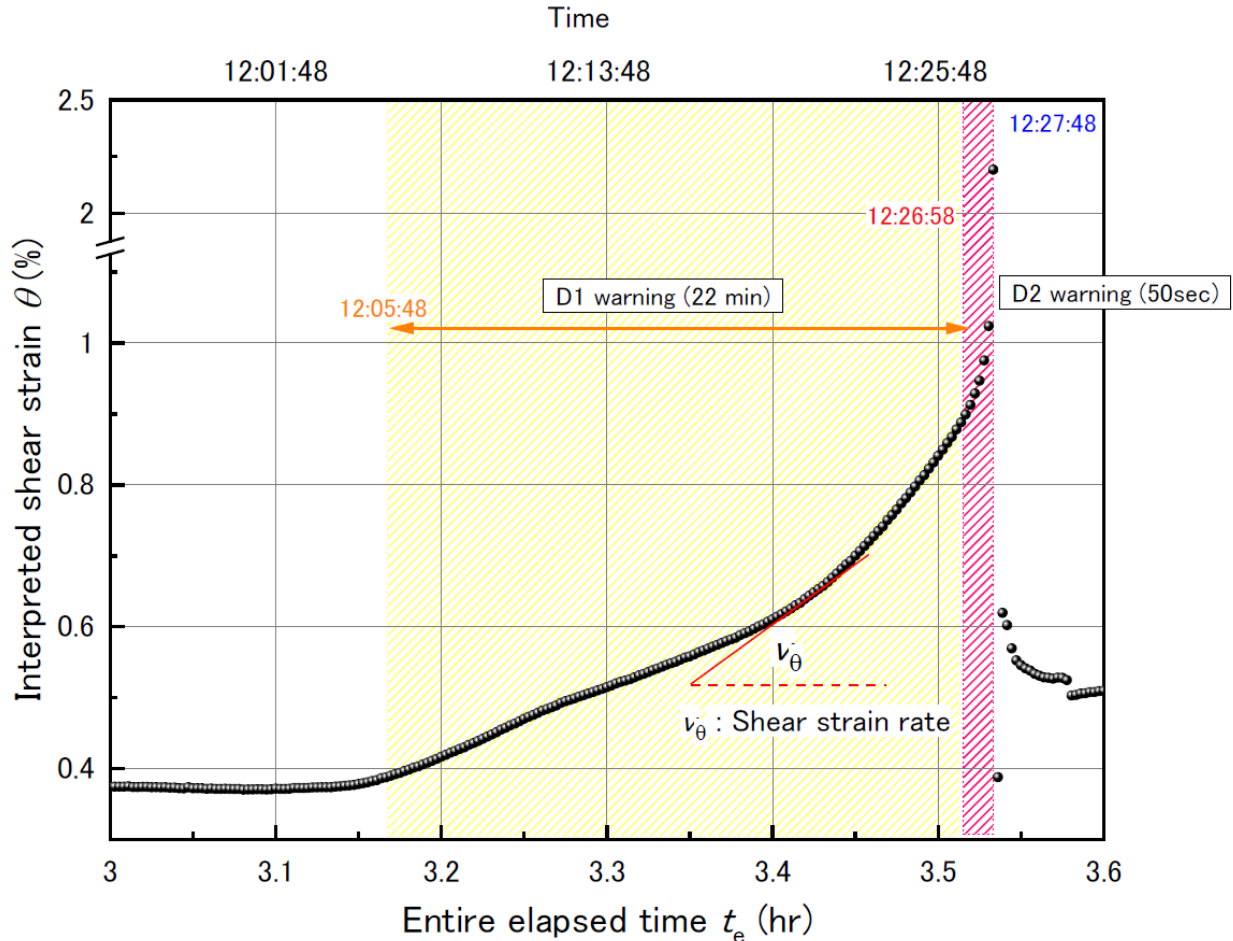


Figure 45. Expanded view of relationship between θ and the elapsed time (t_e) prior to failure.

Figure 46 shows that the relationship between the inverse of the shear strain rate ($|1/v_\theta|$) and the entire elapsed time (t_e). The inverse of the shear strain rate is widely distributed from 0.8 to over 100,000 min/%. A large value of $|1/v_\theta|$ results from a small value of v_θ , even though there was no soil movement during that period. However, the values of $|1/v_\theta|$ decreased to around 100 at the beginning of the second excavation (step 2 to step 4, Figure 17), from 2 to 3 m in depth. This indicates that the soil deformed slightly near the shoulder. Then the values dropped again below 10 at the third excavation (step 5, Figure 17). This was caused by the small failure at the cutting vertical surface, as mentioned earlier.

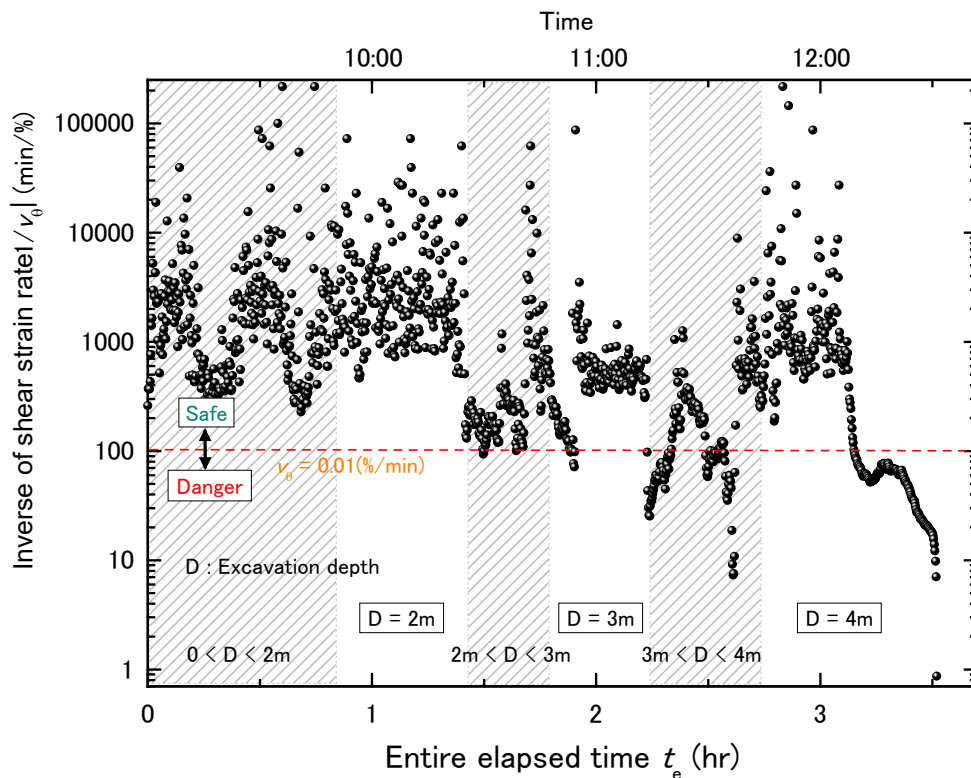


Figure 46. Relationship between inverse of shear strain rate $|1/v_\theta|$ and entire elapsed time t_e .

Higher values of $|1/v_\theta|$, i.e., those over 1,000, were recorded after completion of a series of excavations. Whereas the trench wall was stable from 2.63 to 3.12 hr of t_e , a clear decrease in $|1/v_\theta|$ appeared again after 3.12 hr of t_e .

Figure 47 shows an expanded view of the relationship between the inverse shear strain ($|1/v_\theta|$) and the remaining time prior to failure (t_r). In this chart, zero (0) in t_r means the time of trench failure. Negative values of t_r indicate the remaining time prior to failure. Values of $|1/v_\theta|$ decreased at -23 min in t_r even though no movement could be seen in the video recording. No cracks could be seen on the soil surface in the photos taken until just before failure. However, the MPSM was able to successfully detect the warning signs by measuring small movements in the soil.

The right-hand chart in

Figure 47 shows the decrease in the inverse shear strain ($|1/v_\theta|$) from 25 minutes before failure. After a sharp (drastic) decrease in $|1/v_\theta|$, the values increased slightly and then remained relatively stable within the range of 50 to 80 min/%. This slight increase was similar to the second creep. Accordingly, shear strain θ increased at an almost constant rate between -22 and -10 min of t_r .

However, $|1/v_\theta|$ then declined again from -10 min in t_r . Note that a decrease in $|1/v_\theta|$ means an acceleration of the increase in θ . The curve turned downwards at -50 seconds in t_r , indicating an acceleration of the increase in θ . The MPSM alert system signalled the occurrence of a third creep, which triggered a D2 warning.

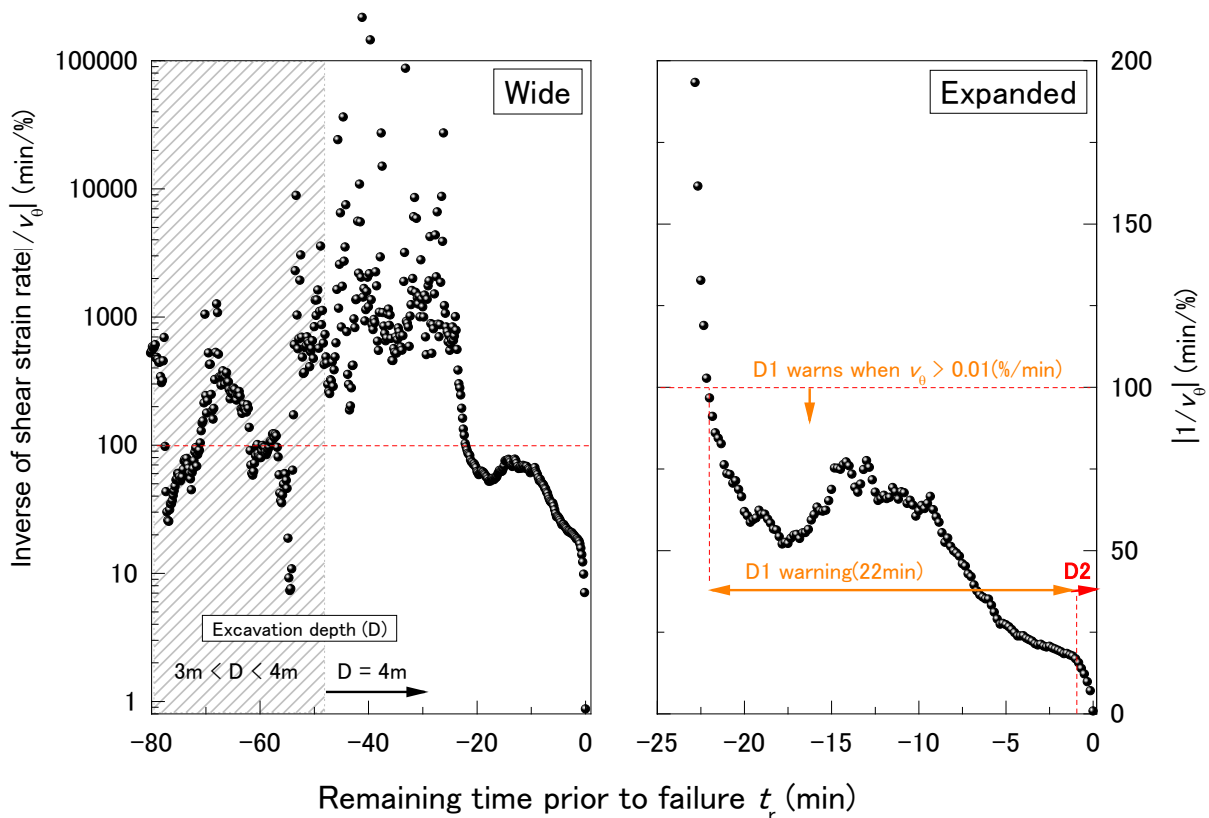


Figure 47. Expanded view of relationship between the inverse shear strain ($|1/v_\theta|$) and the remaining time prior to failure (t_r), for 80 minutes prior to failure (left panel) and for 25 minutes prior to failure (right panel).

7. CONCLUSION AND LIMITATIONS

Based on the test results of trench A1, the MPSM is easy to install on site with a wrench key. The MPSM worked well during site tests in typical Champlain Sea clay. Warnings D1 (yellow light) and D2 (red light) were triggered, indicating an imminent cave-in. D1 appeared 22 minutes prior to cave-in, whereas D2 was triggered 50 seconds prior to the cave-in. Thus, with the MPSM, the increased risk of cave-in during trench excavation could be measured. Based on the positive result obtained when testing with trench A1, the MPSM could have potential for use on Quebec sites in typical Champlain Sea clays for the detection and the warning of imminent trench wall collapse. The current price of an MPSM system is about US\$7,000, according to the JNIOOSH researchers.

Based on the test results obtained with trench A2, the MPSM was able to detect an increase in shear strain, corresponding to the soil settling around the device. The MPSM alarm went off twice, corresponding to the placing of concrete blocks in close proximity to the MPSM sensor. This typical response from the MPSM is expected and the alarm signal usually lasts about one minute, while the soil settles, then stops. No false alarm was detected during the 46 hours that followed the loading of trench A2. Unfortunately, no slope failure occurred in trench A2, which prevented us from assessing the ability of the MPSM to detect the increased risk of slope failure.

Limitations

Further research is required to test the MPSM with other types of Quebec soil and to assess its reliability in Champlain Sea clay. Even though the MPSM works well technically, further testing will also be needed to assess its validity and use within the framework of the *Safety Code for the construction industry*.

A sensitivity study should be conducted for different soil types to assess the influence of the MPSM placement relative to the trench wall. That way, clear indications could be given to the end user as to where to install the MPSM in order to predict soil failure adequately.

The MPSM flexible rod length is fixed at 0.6 m. While laboratory results with Kanto loam (testing at JNIOOSH) seem to indicate that it is enough to measure the creep phenomenon and to predict the soil failure before it happens, this rod length may not be optimal. Indeed, depending on the type of soil and on the failure mechanism, a longer flexible rod may enhance the precision of the MPSM. Therefore, a parametric study should be conducted to assess the performance of the MPSM with a 0.6 m flexible rod length for all of Quebec soil types.

Finally, the current expertise did not assess how the MPSM is susceptible to error. More testing is thus required in order to compute the probability of failure on demand of the device, considering its electronic design and the device location relative to the slope or trench.

REFERENCES

Construction Projects, O Reg 213/91

- Demers, D., & Leroueil, S. (2002). Evaluation of preconsolidation pressure and the overconsolidation ratio from piezocone tests of clay deposits in Quebec. *Canadian Geotechnical Journal*, 39(1), 174-192. doi: 10.1139/t01-071
- Dourlet, S. (2019). *Étude expérimentale de deux excavations à Louiseville*. (Master's thesis, Université Laval, Quebec, QC).
- Fukuzono, T. (1985). A new method for predicting the failure time of a slope. In Japan Landslide Society (Ed.), *Proceedings of the Fourth International Conference and Field Workshop on Landslides* (p. 145–150). Tokyo, Japan: Tokyo University Press.
- Fukuzono, T. (1996). Creep model of Kanto loam and its application to time prediction of landslide. In J. Chacon, C. Irigaray & T. Fernandez (Eds.), *Proceeding of the Eighth International Conference and Field Workshop on Landslides, Granada, Spain* (p. 221-233). Rotterdam, Netherlands: A.A. Balkema.
- Galy, B., LeBoeuf, D., Chaallal, O., & Lan, A. (2021). *Classification des sols et sélection des systèmes d'étalement pour l'excavation des tranchées* (Report No. R-1144-fr). Montreal, QC: IRSST.
- Health and Safety Executive. (1974). *Health and safety at work etc act 1974*. London, England: HSE.
- Jaboyedoff, M., Oppikofer, T., Abellán, A., Derron, M.-H., Loye, A., Metzger, R., & Pedrazzini, A. (2012). Use of LIDAR in landslide investigations: A review. *Natural Hazards*, 61(1), 5-28. doi: 10.1007/s11069-010-9634-2
- Kovacevic, M. S., Car, M., Bacic, M., Stipanovic, I., Gavin, K., Noren-Cosgriff, K., & Kaynia, A. (2018). *Report on the use of remote monitoring for slope stability assessments*. Retrieved from <http://www.destinationrail.eu/ajax/DownloadHandler.php?file=2134>
- Kumar, A., & Villuri, V. G. K. (2015). Role of mining radar in mine slope stability monitoring at open cast mines. *Procedia Earth and Planetary Science*, 11, 76-83. doi: 10.1016/j.proeps.2015.06.010
- Lafleur, J., Chiasson, P., Asselin, R., & Ducharme, A. (1987). *Évaluation des risques pour les travailleurs dans les excavations* (Report No. GEO-87-001). Montreal, QC: École Polytechnique de Montréal.
- Lafleur, J., Silvestri, V., Asselin, R., & Soulié, M. (1988). Behaviour of a test excavation in soft Champlain sea clay. *Canadian Geotechnical Journal*, 25(4), 705-715. doi: 10.1139/t88-081
- Lan, A. (2015). *Analysis of serious/fatal accidents reports of the CNESST in excavation work from 1973 to 2015* [Unpublished report]. Montreal, QC: IRSST.
- Leroueil, S., Hamouche, K., Tavenas, F., Boudali, M., Locat, J., Virely, D., . . . Leblond, P. (2003). Geotechnical characterization and properties of a sensitive clay from Québec. In T.S. Tan, K. K. Phoon, D. W. Hight, & S. Leroueil (Eds.), *Characterisation and engineering properties of natural soils* (p. 363-393). Lisse, Netherlands: Swets & Zeitlinger.

- Manetti, L., & Steinmann, G. (2007). *3DeMoN ROBOVEC: Integration of a new measuring instrument in an existing generic remote monitoring platform*. Paper presented at the Seventh International Symposium on Field Measurements in Geomechanics, Boston, MA. doi: 10.1061/40940(307)91
- Occupational Health and Safety Act, SA 2020, c O-2.2.
- Occupational Health and Safety Regulation, BC Reg 296/97
- National Institute of Occupational Health and Safety, Japan. (2012). *Full scale of experimental test of slope failure*. Tokyo, Japan: JNIO SH.
- Occupational Health and Safety Administration. (1989a). *1926.550: Scope, application, and definitions applicable to subpart P*. OSHA standard No. 1926.550. Washington, DC: OSHA.
- Occupational Health and Safety Administration. (1989b). *1926.651: Specific excavation requirements*. OSHA standard No. 1926.651. Washington, DC: OSHA.
- Occupational Health and Safety Administration. (1989c). *1926.652: Requirements for protections systems*. OSHA standard No. 1926.652. Washington, DC: OSHA.
- Occupational Health and Safety Administration. (1994). *OSHA Part 1926: Subpart P: Excavations*. OSHA standard No. 1926. Washington, DC: OSHA.
- Péloquin, É. (1992). *Étude d'un système de blindage géotextile pour les tranchées de faibles profondeurs*. (Master's thesis, Polytechnique Montréal, Montréal, QC).
- Prokop, A., & Panholzer, H. (2009). Assessing the capability of terrestrial laser scanning for monitoring slow moving landslides. *Natural Hazards and Earth System Sciences*, 9(6), 1921-1928. doi: 10.5194/nhess-9-1921-2009
- Rochelle, P. L., Sarrailh, J., Tavenas, F., Roy, M., & Leroueil, S. (1981). Causes of sampling disturbance and design of a new sampler for sensitive soils. *Canadian Geotechnical Journal*, 18(1), 52-66. doi: 10.1139/t81-006
- Safety Code for the construction industry*, RLRQ, c S-2.1, r. 4.
- Saito, M. (1965). Forecasting the time of occurrence of a slope failure. In *Proceedings of the Sixth International Conference on Soil Mechanics and Foundation Engineering, Montreal, 8-15 September, 1965* (vol. 2, p. 537-541). Toronto, ON: Toronto University Press.
- Tamate, S. (2010). *U.S. Patent No. 7,762,143 B2*. Washington, DC: U.S. Patent and Trademark Office.
- Tamate, S., & Hori, T. (2017). Study on monitoring for detection of potential risk of slope failure for labor safety. In J. Huang, G. A. Fenton, L. Zhang, & D. V. Griffiths (Eds.), *Geo-risk 2017: Impact of spatial variability, probabilistic site characterization, and geohazards* (p. 267-279). Reston, VA: ASCE. doi: 10.1061/9780784480717.025
- Tamate, S., & Hori, T. (2018a). *A combined study of centrifuge and full scale models on detection of threat of failure in trench excavations*. Paper presented at the International Conference on Physical Modelling in Geotechnics, London, England.
- Tamate, S., & Hori, T. (2018b). Monitoring shear strain in shallow subsurface using mini pipe strain meter for detecting potential threat of slope failure. *Geotechnical Testing Journal*, 41(2), 413-424. doi: 10.1520/GTJ20160117
- Tamate, S., Hori, T., Mikuni, C., & Suemasa, N. (2013). Experimental analyses on detection of potential risk of slope failure by monitoring of shear strain in the shallow section. In P. Delage, J. Desrues, R. Frank, A. Puech, & F. Schlosser (Eds.), *Proceedings of the 18th International Conference on Soil Mechanics and Geotechnical Engineering* (p. 1901-1904). Paris, France: Presses des Ponts

- Tamate, S., Suemasa, N., & Katada, T. (2005). Analyses of instability in mobile cranes due to ground penetration by outriggers. *Journal of Construction Engineering and Management*, 131(6), 689-704. doi: 10.1061/(ASCE)0733-9364(2005)131:6(689)
- Wang, M., Liu, K., Yang, G., & Xie, J. (2017). Three-dimensional slope stability analysis using laser scanning and numerical simulation. *Geomatics, Natural Hazards and Risk*, 8(2), 997-1011. doi: 10.1080/19475705.2017.1290696